



**HAL**  
open science

## **Seismic evidence for the presence of Jurassic oceanic crust in the central Gulf of Cadiz (SW Iberian margin)**

Valenti Sallarès, A. Gailler, Marc-André M-A Gutscher, David Graindorge, Rafael Bartolomé, Eulalia Gracia, Jordi Diaz, Juan José Dañobeitia, Nevio Zitellini

### ► **To cite this version:**

Valenti Sallarès, A. Gailler, Marc-André M-A Gutscher, David Graindorge, Rafael Bartolomé, et al. Seismic evidence for the presence of Jurassic oceanic crust in the central Gulf of Cadiz (SW Iberian margin). *Earth and Planetary Science Letters*, 2011, 311 (1-2), pp.112-123. 10.1016/j.epsl.2011.09.003 . insu-00643515

**HAL Id: insu-00643515**

**<https://insu.hal.science/insu-00643515>**

Submitted on 24 Nov 2011

**HAL** is a multi-disciplinary open access archive for the deposit and dissemination of scientific research documents, whether they are published or not. The documents may come from teaching and research institutions in France or abroad, or from public or private research centers.

L'archive ouverte pluridisciplinaire **HAL**, est destinée au dépôt et à la diffusion de documents scientifiques de niveau recherche, publiés ou non, émanant des établissements d'enseignement et de recherche français ou étrangers, des laboratoires publics ou privés.

1 **Seismic evidence for the presence of Jurassic oceanic crust in the**  
2 **central Gulf of Cadiz (SW Iberian margin)**

3

4 Valentí Sallarès<sup>(1,+)</sup>

5 Audrey Gailler<sup>(2,\*)</sup>, Marc-André Gutscher<sup>(2)</sup>, David Graindorge<sup>(2)</sup>, Rafael Bartolomé<sup>(1)</sup>, Eulàlia

6 Gràcia<sup>(1)</sup>, Jordi Díaz<sup>(3)</sup>, Juan José Dañobeitia<sup>(1)</sup>, Nevio Zitellini<sup>(4)</sup>

7

8 <sup>(1)</sup> Unitat de Tecnologia Marina-CSIC, Barcelona, Spain

9 <sup>(2)</sup> Université de Brest, Laboratoire Domaines Océaniques, UMR6538 CNRS/UBO, IUEM,  
10 Plouzané, France

11 <sup>(3)</sup> Institut de Ciències de la Terra “Jaume Almera” (ICTJA), Solé i Sabaris, Barcelona, Spain

12 <sup>(4)</sup> Istituto di Scienze Marine (ISMAR)-CNR, Bologna, Italy

13 <sup>(\*)</sup> now at Commissariat d’Energie Atomique, DAM/DIF, F-91297 Arpajon, France

14

15 <sup>(+)</sup> Corresponding author:

16 Valentí Sallarès

17 Unitat de tecnologia Marina (UTM)

18 Consejo Superior de Investigaciones Científicas (CSIC)

19 Passeig Marítim de la Barceloneta 37-49

20 08003 – Barcelona (Spain)

21

22 Email: [vsallares@cmima.csic.es](mailto:vsallares@cmima.csic.es)

23 Phone: +34 – 932 309 623

24 Fax: +34 – 932 309 555

25 **Abstract**

26

27         We investigate the crustal structure of the SW Iberian margin along a 340 km-long  
28 refraction and wide-angle reflection seismic profile crossing from the central Gulf of Cadiz to  
29 the Variscan continental margin in the Algarve, Southern Portugal. The seismic velocity and  
30 crustal geometry model obtained by joint refraction and reflection travel-time inversion  
31 reveals three distinct crustal domains: the 28-30 km-thick Variscan crust in the north, a 60  
32 km-wide transition zone offshore, where the crust abruptly thins ~20 km, and finally a ~7 km-  
33 thick and ~150 km-wide crustal section that appears to be oceanic in nature. The oceanic crust  
34 is overlain by a 1-3 km-thick section of Mesozoic to Eocene sediments, with an additional 3-4  
35 km of low-velocity, unconsolidated sediments on top belonging to the Miocene age, Gulf of  
36 Cadiz imbricated wedge. The sharp transition between continental and oceanic crust is best  
37 explained by an initial rifting setting as a transform margin during the Early Jurassic that  
38 followed the continental break-up in the Central Atlantic. The narrow oceanic basin would  
39 have formed during an oblique rifting and seafloor spreading episode between Iberia and  
40 Africa that started shortly thereafter (Bajocian) and lasted up to the initiation of oceanic  
41 spreading in the North Atlantic at the Tithonian (late Jurassic-earliest Cretaceous). The  
42 velocity model displays four wide, prominent, south-dipping low-velocity anomalies, which  
43 seem to be related with the presence of crustal-scale faults previously identified in the area,  
44 some of which could well be extensional faults generated during this rifting episode. We  
45 propose that this oceanic plate segment is the last remnant of an oceanic corridor that once  
46 connected the Alpine-Tethys with the Atlantic ocean, so it is, in turn, one of the oldest  
47 oceanic crustal fragments currently preserved on Earth. The presence of oceanic crust in the  
48 central Gulf of Cadiz is consistent with geodynamic models suggesting the existence of a  
49 narrow, westward retreating oceanic slab beneath the Gibraltar arc-Alboran basin system.

50

51 **1. Introduction**

52

53 The region offshore SW Iberia lies at the eastern end of the Azores-Gibraltar fracture zone  
54 (AGFZ), and is part of the complex plate boundary between the African and Eurasian plates  
55 (Figure 1). The tectonic behavior along the AGFZ is complex, varying from extensional in the  
56 West, close to the Mid-Atlantic Ridge, strike-slip in the center, along the Gloria fault, and  
57 mostly compressional in the East, from cape São Vicente to the Strait of Gibraltar. The  
58 regional tectonic history has been dominated by the long-term evolution of the triple junction  
59 between the North-American, African and Eurasian plates, as well as the interaction with  
60 other smaller blocks such as the Iberian plate (e.g. Srivastava et al., 1990; Olivet, 1996). Plate  
61 kinematic models and GPS observations show that Africa is currently moving in a NW-WNW  
62 direction with respect to Iberia at 4-5 mm/yr (Argus et al., 1989; Nocquet and Calais, 2004).  
63 This plate boundary is fairly diffuse, marked by an E-W trending band of seismicity about  
64 100-200 km wide (e.g. Bufo et al., 1995). Moderate to strong earthquakes have struck here  
65 in the past, with a combination of compressional and strike-slip focal mechanisms (Grimison  
66 and Chen, 1986; Stich et al., 2003; 2006). In addition to this continuous, moderate magnitude  
67 seismic activity, the region has been also struck by large historical earthquakes, most notably  
68 the catastrophic Great Lisbon earthquake of 1755 ( $M_w=8.5-8.6$ ) (Johnston et al., 1996).

69 A major limit exists in the Gulf of Cadiz between the Central Atlantic domain, which  
70 opened in the Early Jurassic, and the Northern Atlantic domain, which opened in the Upper  
71 Cretaceous (e.g., Roest and Srivastava, 1991; Olivet, 1996; Rovere et al., 2004; Sahabi et al.,  
72 2004). Available plate reconstruction models suggest that the region might have been the site  
73 of limited amounts of oceanic spreading due to the ESE migration of the African plate with  
74 respect to Iberia during this period of time (e.g. Stampfli and Borel, 2002; Schettino and

75 Turco, 2011). The possible presence of an oceanic basin of Jurassic age in this area is a  
76 largely debated question that has profound implications in the geodynamic evolution of the  
77 Western Mediterranean, and most specifically the Alboran basin system (e.g. Lonergan and  
78 White, 1997; Gutscher et al., 2002; Faccenna et al., 2004). Unfortunately, the nature of the  
79 crust in the deep oceanic domains offshore SW Iberia is unknown and difficult to determine  
80 because there are few recognizable magnetic anomaly patterns (Verhoef et al., 1991), and the  
81 seafloor is covered by a thick layer of Mesozoic to recent sediments, thus basement samples  
82 are difficult to obtain. The only deep sea drilling in the region that penetrated to the basement  
83 was the DSDP site 120 on Gorringer Bank (Figure 1), where serpentinized peridotite  
84 corresponding to exhumed mantle, gabbro, and extrusive rocks were sampled (Ryan et al.,  
85 1973). Similar rocks were also recovered during dredging and deep-sea submersible  
86 expeditions (Auzende et al., 1984; Girardeau et al., 1998). DSDP site 135 Southwest of the  
87 Coral Patch Ridge (Figure 1) penetrated Jurassic sediments (Aptian) but did not reach the  
88 basement (Hayes et al., 1972). Finally, continental rocks of Paleozoic age have been also  
89 sampled at the Guadalquivir Bank in the Iberian margin (Malod and Mougenot, 1979).  
90 Because of the lack of basement samples, current knowledge of the crustal domains in the  
91 Gulf of Cadiz is based almost exclusively on geophysical data. Available multi-channel  
92 seismic (MCS) data (Sartori et al., 1994; Banda et al., 1995; Torelli et al., 1997; Gràcia et al.,  
93 2006), as well as refraction and wide-angle reflection (WAS) data (Purdy, 1975; González et  
94 al., 1996; Gutscher et al., 2002) and models based on potential field data (e.g. Gràcia et al.,  
95 2003; Fullea et al., 2010), globally highlight the eastward increase in sediment thickness,  
96 depth to basement, and depth to Moho (Iribarren et al., 2007; Gutscher et al., 2009b), but do  
97 not provide information on the crustal nature across the different tectonic boundaries.

98 In fall 2008, in the framework of the EU-funded NEAREST (NEAR shore sources of  
99 Tsunamis: towards an early warning system) project, the NEAREST-SEIS WAS survey was

100 performed in the Gulf of Cadiz. During that survey, two long profiles using Ocean Bottom  
101 Seismometers (OBS) and land stations were acquired to probe the deep structure of the SW  
102 Iberian margin and adjacent oceanic areas (Figure 1). One of the profiles was mainly designed  
103 to shed light on the unresolved question of the crustal nature in the central Gulf of Cadiz (N-S  
104 profile in figure 1). The interpretation of the modeling results obtained along this profile,  
105 which begins in the Seine Abyssal Plain, crosses the Gulf of Cadiz imbricated wedge (GCIW)  
106 and several of the “SWIM” lineaments (Zitellini et al., 2009), the Portimao bank, and  
107 continues up onto the Portuguese continental shelf until the Variscan Iberian domain, are the  
108 main goals of the work presented in this paper.

109

## 110 **2. Data acquisition**

111

112 The WAS data were acquired onboard the Spanish R/V Hesperides. Fifteen OBS were  
113 deployed along a 257-km-long shooting line reaching from the southern tip of the GCIW into  
114 the Portimao Canyon (Figure 1). Four of the OBS were L-Cheapo 4x4 instruments, designed  
115 by the Scripps Institution of Oceanography, and belonging to the Spanish OBS pool operated  
116 by the UTM-CSIC. The other eleven OBS were from the joint IFREMER-IUEM pool  
117 (Auffret et al., 2004). The profile was extended on land in Portugal by 7 land-stations. Due to  
118 timing problems we used only 3 of these stations in the modelling, giving a total recording  
119 length of 342 km. The source was composed of 7 airguns organized in two arrays, providing a  
120 total volume of 4320 c.i. The arrays were deployed at a depth of 12 m, and the shot interval  
121 was set to 90 s (~210 m) to avoid noise generated by previous shots. Pre-processing of the  
122 OBS data included calculation of the clock-drift corrections and instrument relocation for  
123 spatial drift during their fall to the seafloor.

124 Most of the WAS data have a good quality, showing clear sedimentary (Ps) and intra-

125 crustal refracted phases (Pg), reflections at the sediment-basement interface (PsP) and crust-  
126 mantle boundary (PmP), and deeper arrivals refracted in the upper mantle (Pn) up to 100 km  
127 offset in some OBS, and to more than 150 km in the land stations. Five of the record sections  
128 at OBS and land stations are displayed in figure 2.

129         Seismic sections of the instruments located on the top of the GCIW show clear low-  
130 velocity sedimentary refractions (Ps) and reflections at the top of the basement (PsP).  
131 Significant variations are observed between record sections of the southern instruments,  
132 located towards the frontal part of the GCIW, and those located northward in the Algarve  
133 basin area (Figure 2d). Seismic sections from OBS located close to the Portimao canyon in  
134 very shallow water have limited quality. Conversely, long offset PmP and Pn phases can be  
135 clearly traced on the record sections of all the land stations (Figure 2e). Instruments located  
136 southward, in deeper water show clearer arrivals, including sediment and crustal arrivals  
137 (Figure 2a). In the modelling of the crustal structure we used data recorded at all the OBS and  
138 at the three land stations located the closest to the coast (Figure 1).

139

### 140 **3. Travel-time picking and modelling approach**

141

142         A total of 4003 picks, including first arrivals (Ps, Pg, Pn) and secondary reflections  
143 (PsP and PmP) were identified in the record sections. Picking was done manually on  
144 unfiltered data where possible and if needed, a deconvolution whitening, band-pass filtering  
145 (4-16 Hz) and Automatic Gain Correction were applied to improve lateral coherence and  
146 increase signal-to-noise ratio. Ps and PsP phases were observed and picked in all the OBS  
147 located on top of the sedimentary wedge, and Pg was also observed to variable offset in all the  
148 OBSs. PmP and Pn's could not be identified in all the record sections, especially in the two  
149 shallowest, northernmost OBSs. A picking uncertainty was assigned to the different picks

150 taking into account the quality of the phase, individual picking errors, and a possible  
151 systematic shift, of the order of half of the dominant period of the dominant signal, in the  
152 arrival identification. For Ps and near-offset Pg phases the average assigned uncertainty was  
153 40-50 ms, while it was 60-70 ms for far-offset Pg's and 70-80 ms for Pn's. For PsP reflections  
154 it was 50-60 ms, and 70-80 ms for PmP's.

155 The 2-D velocity-depth model was obtained using the *tomo2d* joint refraction and  
156 reflection travel-time inversion code described in Korenaga et al. (2000). The method allows  
157 inverting simultaneously and independently travel-times from first arrivals and from a  
158 reflected phase, to obtain a velocity model and the geometry of a floating reflector. Travel-  
159 times and ray paths are calculated using a hybrid ray-tracing scheme based on the graph  
160 method (Moser et al., 1991) and a local ray bending refinement. Smoothing constraints for  
161 predefined correlation lengths and optimized damping for the model parameters are used to  
162 regularize the iterative linearized inversion (see Korenaga et al., 2000, for details).

163 To perform the inversion we employed an original multi-step, hybrid inversion  
164 strategy consisting of (1) splitting the data into two subsets, one for instruments located on the  
165 sedimentary wedge, and the other for those in the continental margin, and (2) adding the data  
166 sequentially, starting from the shortest offsets/uppermost levels, and finishing with the longest  
167 offsets/deepest levels.

168 The velocity model for the southern part of the profile was constructed in two steps,  
169 corresponding to the inversion of the sediments and crust. The Ps and PsP phases were used  
170 to invert for the velocities and thickness of the sedimentary wedge, and hence the geometry of  
171 the sediment-basement boundary (Figure 3a and 3b). The starting model was a laterally-  
172 extended "minimum 1-D velocity model", which is the one that fits the best the Ps travel-  
173 times (e.g. Sallarès et al., 2003). The top of the basement reflector was initially set at 7 km.  
174 The inverted velocity model of the sediments was included as a priori information in the



175 second inversion step, in which Ps, Pg and PmP arrivals were used to obtain the crustal  
176 velocity distribution and Moho geometry. The sediment velocity parameters were over-  
177 damped by a factor of 20 to 1 to let the inversion modify the model preferably within the  
178 crust. The starting velocity model below the sediment layer was a 1-D model varying  
179 uniformly from 4.5 km/s at the sediment-basement boundary to 7.2 km/s 7 km below,  
180 simulating an Atlantic oceanic crust older than 140 m.y. (White et al., 1992). The initial Moho  
181 reflector was set 7 km below the sediment-basement boundary. The corresponding 2-D crustal  
182 velocity model, obtained after 8 iterations, is shown in figures 3c and 3d.

183         The velocity model for the northern part of the profile was inverted in a single step,  
184 since no clear Ps or PsP phases were identified in the record sections. Consequently,  
185 sediments and crust were inverted together using the Pg and PmP phases to model the crustal  
186 velocity field and Moho geometry. The 2-D starting velocity model was constructed  
187 combining a 1-D model for the offshore section (i.e., the model that best fits Pg arrivals from  
188 the OBS located in the Algarve basin), and a second one for the onshore section, which was  
189 extracted from an onshore WAS profile acquired nearby (Palomeras et al., 2009). At the land-  
190 sea transition, the seismic velocities of the reference model were calculated by linear  
191 interpolation of these two 1-D velocity-depth models. The 2-D crustal velocity model for the  
192 northern section obtained after 8 iterations is shown in figures 3e and 3f.

193         In the third and last step, the southern and northern crustal models were merged  
194 together and a new inversion was performed using the whole set of refractions (Ps, Pg, and Pn)  
195 together with PmP's, to obtain a complete model including sediments, crust and uppermost  
196 mantle along the entire profile. As in the previous steps, the velocity nodes above the basal  
197 reflector were over-damped to favour model changes below the Moho. Beneath the Moho, a  
198 laterally-extended 1-D velocity-model with velocity varying uniformly from 7.5 km/s below  
199 the Moho to 8.3 km/s at 35 km depth, although alternative models with higher velocity

200 beneath the Moho were also tested. The 2-D velocity model obtained after 7 iterations is  
201 shown in figure 4. The final rms for this model is 65 ms ( $\chi^2=1.02$ ), with an rms of 61 ms for  
202 first arrivals and 72 ms for PmP's. The derivative weight sum (DWS), which is the column  
203 sum vector of the velocity kernel (Toomey and Foulger, 1989) and provides information on  
204 the linear sensitivity of the inversion, is shown in figure 5a.

205

## 206 **4. Results**

207

### 208 ***4.1. Seismic structure***

209 The final velocity model in figure 4 shows marked differences between the  
210 sedimentary and crustal structures from south to north, with a marked transition zone between  
211 160 and 210 km distance along the profile where the crust thins sharply. The southern part of  
212 the model (0-160 km along profile), which runs across the GCIW, shows a ~5 km thick layer  
213 corresponding to the sedimentary cover, with velocities ranging from ~1.8 km/s at the top to  
214 ~3.5 km/s at the base. This layer can in turn be subdivided in an upper layer of 2-3 km with  
215 velocity between ~1.6 km/s and 3.0 km/s, and a bottom one of 1-2 km with velocity between  
216 2.8 km/s and 4.0 km/s. This sedimentary unit exhibits a quite uniform thickness along the  
217 southern 120 km of the profile, then thins progressively to the north, and more abruptly  
218 landward from ~125 km (between OBS37 and 38).

219 The crust below the sedimentary units shows a rather uniform thickness of ~7.0 km  
220 between 0 km and 160 km. Crustal velocities vary from 4.6-4.8 km/s at the top to 6.9-7.1  
221 km/s at the base. The vertical velocity gradient is steeper in the uppermost crust (~0.45 s<sup>-1</sup> in  
222 the upper 2 km) than in the lower part (~0.14 s<sup>-1</sup> in the lower 5 km) (Figure 4). The Moho  
223 depth and geometry is constrained by PmP reflections, and it follows the basement  
224 topography along most of the section. The long-wavelength crustal velocity field is rather

225 uniform laterally, except for a pronounced anomaly centred at 130-145 km (between OBS38  
226 and 39), as indicated by the depression of the velocity contours observed in this area (Figure  
227 4) that gets down to the Moho but does not affect the sediments. The anomaly is clearly  
228 imaged in figure 6 representing the negative anomalies with respect to a laterally-smoothed  
229 velocity average along the profile. As it is observed in this figure, the corresponding anomaly  
230 (f1) has an amplitude of -0.5 km/s, dips to the south, and is >10 km-wide. A second crustal-  
231 scale low-velocity anomaly with similar geometry but lower amplitude ( $\sim$ -0.15 km/s) was  
232 also detected at  $\sim$ 90 km (f0 in figure 6).

233         The profile section between 160 and 210 km (between OBS41 and 44) corresponds to  
234 the rough topographic region between the GCIW and the Algarve Basin. This segment  
235 accommodates almost all the crustal thickening. Within  $\sim$ 60 km, the Moho deepens from  $\sim$ 14  
236 km to  $\sim$ 25 km depth (corresponding to a slope of  $\sim$ 12-13 $^\circ$ ), so the crust thickens drastically  
237 from  $\sim$ 7 km to  $\sim$ 24 km. Northward from 210 km the vertical velocity gradient decreases  
238 ( $\sim$ 0.05 s $^{-1}$ ), reaching maximum velocities of 6.9-7.0 km/s just above the crust-mantle  
239 boundary. The Moho geometry in this section is mainly constrained by PmP arrivals (OBS44  
240 in figure 2d). The shallow velocity field at the transition zone from the oceanic domain  
241 towards the continent indicates the presence of a thin sediment cover on top of the basement,  
242 so that Ps/PsP phases are not distinguished in the record sections, so that the structure of the  
243 sedimentary layers and the sediment-basement interface could not be properly defined. In this  
244 area, two bathymetric highs are present, one located at  $\sim$ 180 km (the Portimao Bank) and the  
245 other one located at 200-210 km (a spur bounding the Portimão canyon). The isovelocity  
246 contour of 4.0 km/s reaches there almost the surface, indicating that the basement is possibly  
247 outcropping here (BH in Figure 1). Two zones of relatively low crustal velocity, similar to  
248 that described in the southern part of the model, can be seen at  $\sim$ 180-190 km (between OBS42  
249 and 43) and  $\sim$ 225 km (around OBS44) (Figure 5). Both features are also reflected as

250 pronounced, south-dipping, negative velocity anomalies of up to -0.7 km/s that seem to start  
251 at the seafloor and reach a maximum depth of 13-14 km (f2 and f3 in figure 6). Similarly to  
252 f1, f2 and f3 extend laterally to >10 km in the model and show dip angles of 35-45°.

253 The northernmost part of the model, between 210 km and the end of the profile  
254 (Figure 4), corresponds to the upper part of the contouritic drift and shelf and the Algarve  
255 Basin, characterized by the Variscan basement. It shows only a residual sedimentary cover  
256 that is less than 1 km-thick. In this area the Moho gently deepens from ~25 km at 210 km  
257 along profile (between OBS43 and 44) to ~29 km at 260 km (north from OBS45 in figure 1).  
258 A maximum crustal thickness of 29 km is obtained at the coastline, where crustal velocity  
259 ranges from ~4.8 km/s and ~7.1 km/s. The velocity field in this area is mainly constrained by  
260 the PmP phases recorded in the land stations, so there is a trade-off between lower crustal  
261 velocity and Moho location. The upper mantle is sampled by Pn phases only a few kilometres  
262 below the Moho, and the obtained velocity appears to be considerably low for upper mantle  
263 (7.6-7.7 km/s).

264

#### 265 **4.2 Uncertainty analysis**

266 In order to estimate model parameters uncertainty owing to a combination of data  
267 picking errors and other non-linear effects related to the theoretical approximations made, the  
268 starting model selected, and the experiment geometry, we performed a Monte Carlo-type  
269 stochastic error analysis. The approach followed is similar to that described in Sallarès et al.  
270 (2005) and Gailler et al. (2007), which is a modified version of that of Korenaga et al. (2000),  
271 and consists of: (1) generating a set of 250 2-D starting models by randomly perturbing  
272 velocity and reflector depth in the initial models within reasonable bounds, which are chosen  
273 according to *a priori* lithological information. In our case we have used the resulting model  
274 shown in figure 4 as reference. Velocities have been varied within  $\pm 0.35$  km/s in crust and

275 mantle, and Moho geometry within  $\pm 1.25$  km in the oceanic domain and within  $\pm 2.5$  km in  
276 the continent. In addition, 250 noisy data sets have been generated by adding random timing  
277 errors of  $\pm 60$  ms, including common phase errors ( $\pm 30$  ms), common receiver errors ( $\pm 10$   
278 ms), and individual picking errors ( $\pm 20$  ms), to the reference data set, constituted by first  
279 arrivals and PmPs. Then, we repeated the inversion for 250 randomly selected perturbed  
280 velocity models-noisy data set pairs, using the same inversion parameters as with the model  
281 shown in figure 4. According to Tarantola (1987), the mean deviation of all realizations of  
282 such an ensemble can be interpreted as a statistical measure of the model parameters  
283 uncertainty. The mean deviation of model parameters is shown in figure 5b. The average rms  
284 of all the Monte-Carlo realizations diminishes from 361 ms ( $\chi^2=36.2$ ) before the inversion, to  
285 63 ms ( $\chi^2=1.1$ ) after the inversion.

286         Uncertainty within the sedimentary layer is low ( $\leq 0.1$  km/s), increasing to  $\sim 0.15$  km/s  
287 near the top of the basement, due to the sharp velocity contrast between sediments and  
288 basement and to the strong velocity gradient in the upper part of the crust (e.g. Calahorrano et  
289 al., 2008). Velocity uncertainty within the oceanic crust is also low ( $\leq 0.1$  km/s), confirming  
290 that the crustal velocity field obtained in the oceanic domain of the model is remarkably well  
291 constrained by the data. The Moho geometry in this oceanic domain has an average  
292 uncertainty of less than  $\pm 0.5$  km (Figure 5b).

293         The transitional and continental domains (between 160 km and the end of the model)  
294 also display rather low crustal velocity uncertainty, increasing from  $\leq 0.15$  km/s in average in  
295 the upper third of the crust to  $\sim 0.20$  km/s near the Moho boundary. This locally high  
296 uncertainty reflects the lack of multi-fold ray coverage in this area, especially in the deep part  
297 of the model sampled only by PmP phases, which are subject to trade-off between the  
298 reflector location and the velocity field above it (e.g. Korenaga et al., 2000; Sallarès et al.,  
299 2005). Interestingly, Moho depth uncertainty in the continental domain is reasonably low,

300 varying between  $\pm 1.0$  km in the transition zone, and  $\pm 1.5$  km beneath the coast line, in the  
301 deepest part of the model (Figure 5b).

302 The worst-resolved part of the model corresponds to the upper mantle, where  
303 uncertainty is locally  $\geq 0.2$  km/s. A common problem in WAS experiments is that the low  
304 mantle velocity gradient makes that Pn phases do not dive deep into the mantle (see DWS plot  
305 in figure 5a), so they only carry limited information on the velocity structure of the uppermost  
306 few km of the mantle (e.g., Sallarès and Ranero, 2005). In order to test the reliability of the  
307 obtained upper mantle velocity, we performed two additional inversions using the same  
308 reference crustal velocity model and data set, but including two end-member uppermost  
309 mantle velocities of 7.4 km/s and 8.1 km/s. Both models converged to low mantle velocity  
310 ranging between  $\sim 7.5$  km/s and  $\sim 7.8$  km/s, respectively. Given that the upper mantle is  
311 covered only by Pn to a few km below the Moho, which have a very limited azimuthal  
312 coverage and have a limited penetration, the model parameter resolution at the upper mantle  
313 is low, so that the velocity represents an average along the ray path.

314

## 315 **5. Discussion**

316

### 317 *5.1. Nature of the crustal domains offshore SW Iberia*

318 The final velocity model of figure 4 reveals the presence two distinct crustal domains  
319 (labelled 1 and 2 in our interpretative model of figure 7, summarizing our main structural  
320 interpretations), with a transition zone in between. In domain 1 the crust is  $\sim 7.0$  km thick. It is  
321 overlain by a 1-2 km of high-velocity sediments, and by other 3-4 km of lower-velocity  
322 sediments. These two sedimentary units had been previously identified in different local MCS  
323 profiles over the GCIW (Tortella et al., 1997; Torelli et al., 1997; Gràcia et al., 2003;  
324 Gutscher et al., 2009a). According to these authors the lower unit is constituted by Mesozoic

325 to Eocene sedimentary rocks, whereas the upper one includes the GCIW, mainly emplaced  
326 during Late Miocene, and a thin layer of Upper Miocene to plio-Quaternary sediments that  
327 overlay the GCIW. However, the interpretations regarding the evolution and tectonic behavior  
328 of both units differ in several aspects. A number of authors have suggested that the GCIW is  
329 an allocthonous body emplaced tectonically by the westward migration of the Gibraltar  
330 arc between ~15 Ma and ~8 Ma (e.g. Torelli et al., 1997; Gràcia et al., 2003; Medialdea et  
331 al., 2004; Iribarren, 2009), whereas Gutscher et al. (2009b) consider that this unit is as an  
332 actively deforming accretionary prism on top of an eastward-subducting oceanic slab,  
333 source of the largest earthquakes having occurred in the region. There is however overall  
334 agreement in that the lowermost unit covering the basement is Mesozoic in age (e.g. Sartori et  
335 al., 1993; Torelli et al., 1997; Tortella et al., 1997; Gràcia et al., 2003), giving an upper bound  
336 for the age of the basement below.

337 Domain 2 corresponds to the stable continental Variscan margin of SW Iberia, and  
338 consists of a continental crust (27-30 km thick) overlain by a poorly contrasted sedimentary  
339 layer made of Mesozoic units (Terrinha et al., 2003). The velocity structure and crustal  
340 thickness are very similar to that modelled along the on-shore IBERSEIS WAS transect  
341 (Palomeras et al., 2009), and it is also consistent with that of González et al. (1996), which is  
342 based on land recordings of the IAM data. The transition zone in between both domains is  
343 roughly 60 km-wide, across which occurs an abrupt lateral variation in crustal thickness  
344 between the continental margin and the central Gulf of Cadiz. The sharpest transition takes  
345 place at km 160-170 (marked by “COB” in figure 7).

346 Concerning the nature of the crust in domain 1, there are in principle three possible  
347 interpretations; namely thinned continental crust, exhumed mantle or oceanic crust. Available  
348 heat flow data above the GCIW indicate values from 59-45 mW/m<sup>2</sup> (Grevemeyer et al.,  
349 2008), values that are consistent with old lithosphere but do not help constraining the crustal

350 type. Some ENE-WSW trending magnetic anomalies are also present in the internal Gulf of  
351 Cadiz (Verhoef et al., 1991; Dañobeitia et al., 1999), but these are too subdued and sparse to  
352 be identified as seafloor spreading anomalies. In the absence of direct basement samples or  
353 well-defined magnetic anomalies, the best available indicator on the nature of the crust is the  
354 velocity structure and crustal thickness provided by offshore WAS data. Figure 8 shows a  
355 comparison of 1-D velocity-depth profiles representative of the two crustal domains and the  
356 transition zone with compilations made for: (1) exhumed mantle sections along the western  
357 Iberian margin (Srivastava et al., 2000), (2) >140 m.y.-old Atlantic oceanic crust (White et al.,  
358 1992), (3) continental crust (Christensen and Mooney, 1995), and (4) altered oceanic crust  
359 near subduction trenches (Meléndez et al., 2009). A comparison of the velocities obtained in  
360 domain 1 to velocities of exhumed/serpentinized upper mantle (Figure 8a) show that crustal  
361 velocities are far too slow and velocity gradients too smooth to correspond to exhumed  
362 mantle. In contrast, the obtained velocities are too high to correspond to extended continental  
363 crust (Figure 8a). An additional observation that helps to rule out this option of continental  
364 crustal affinity is that all the continental thinning occurs in domains 2 and 3, and there is no  
365 thinning at all in domain 1 for more than 150 km, an observation that is hardly compatible  
366 with an extended continental nature.

367         The comparison with the velocity structure for >140 m.y.-old Atlantic oceanic crust  
368 (White et al., 1992) is shown in figure 8b. The velocity structure in domain 1 is closer to  
369 oceanic crust than to the two options shown in figure 8a, but it is near the lower velocity  
370 bound. This atypical velocity profile may be the result of fault-related rock fracturing and  
371 subsequent alteration by fluids percolating through faults at this anomalously old (probably of  
372 Jurassic age, see introduction and explanation below), and hence cold and brittle crust. The  
373 presence of low velocity anomalies that spatially coincide with two of the long, N120°E  
374 trending strike-slip “SWIM lineaments”, interpreted by Zitellini et al. (2009) as crustal-scale



375 faults, would support this hypothesis. Anomaly f1 (figure 6) corresponds to the location of the  
376 northernmost lineament (LN in figure 1), whereas f0 is located next to the southern one (LS in  
377 figure 1). Additionally, the uppermost mantle velocity is low, which might be indicative of  
378 mantle serpentinization, probably by means of fluids percolating through the aforementioned  
379 faults crossing the Moho. The low crustal and upper mantle velocity is a common feature in  
380 the oceanic plate at subduction zones. It has been described for the incoming plate in Chile  
381 (Ranero and Sallarès, 2004; Lefeldt et al., 2009) and Middle America (Ivandić et al., 2009;  
382 Meléndez et al., 2009). It has been associated to the presence of pre-existing lithospheric-  
383 scale normal faults that are reactivated by flexure at the outer rise allowing the water to  
384 percolate through the crust well into the upper mantle (Ranero et al., 2003). To check this  
385 hypothesis, we have included in figure 8b a 1-D velocity-depth profile extracted from a WAS  
386 profile acquired in the outer rise area of the Nicaraguan margin (Meléndez et al., 2009).  
387 Clearly, this is the velocity profile that fits the best our model, suggesting that the crust in the  
388 central Gulf of Cadiz could well be a fragment of fractured, altered and serpentinized oceanic  
389 lithosphere. As expected, domains 2 and 3 (Figure 8c and 8d) show 1-D velocity-depth  
390 profiles that fit well within the range of extended and normal continental crust velocities  
391 (Christensen and Mooney, 1995). According to these observations continent-ocean boundary  
392 (COB) is located at the northern limit of domain 1, some 100 km south from the coast line  
393 (Figure 7).

394

## 395 ***5.2. Origin and tectonics of the SW Iberian and NW African margins***

396 The study area is located at the intersection of the NW African and the SW Iberian  
397 continental margins. The NW African margin developed during Triassic-Jurassic times (Le  
398 Roy and Piqué, 2001), as the Central Atlantic formed by the rifting of Africa from North  
399 America at the southern end of the modern day Grand Banks of Newfoundland by extension

400 by transcurrent motion along the current southern Grand Banks fault (Bill et al., 2001;  
401 Stampfli and Borel, 2002) (Figure 9). The SW Iberian margin and the Gulf of Cádiz domain  
402 developed at the intersection of a N-S trending margin, between the West Iberia and the  
403 Flemish Cap - Grand Banks Margin of Newfoundland (Canada), and the Grand Banks  
404 transform referred to above (Roest and Srivastava, 1991). According to reconstructions based  
405 on available plate tectonic models (Stampfli and Borel, 2002; Schettino and Turco, 2011) this  
406 domain may have been the site of limited amounts of oblique seafloor spreading that  
407 accommodated the ~N-S component of the migration of Africa with respect to Eurasia during  
408 the Jurassic. This spreading could have opened a narrow oceanic basin separating southern  
409 Iberia from NW Africa (Figure 9). These reconstructions indicate that the oceanic spreading  
410 between Africa and Iberia would have been coeval with the opening of the Central Atlantic,  
411 starting in the Bajocian (Middle Jurassic) at ~180 Ma (Roeser et al., 2002) and finishing with  
412 the onset of rifting at the North Atlantic in the Tithonian (latest Jurassic), some 145 Ma  
413 (Stampfli and Borel, 2002; Schettino and Turco, 2011).

414         Our work provides the first direct evidence for the presence of oceanic crust between  
415 North Africa and SW Iberia. According to this interpretation, the oceanic crustal section  
416 imaged in figure 4 would represent the westernmost segment of the Alpine-Tethys ocean, the  
417 pre-Alpine oceanic domain that opened between NW Africa and Eurasia in the Jurassic and  
418 closed during the Alpine orogeny (Stampfli and Borel, 2002; Schettino and Turco, 2011;  
419 Handy et al., 2010). A south-eastern branch of this oceanic domain is the true Tethys, which  
420 was consumed by north-dipping subduction as Africa converged northward with Europe, a  
421 process which continues today beneath the Hellenic and Calabrian arcs (e.g. Faccenna et al.,  
422 2001). Therefore, the Alpine-Tethys domain represented the boundary zone between the  
423 Atlantic and Tethys domains during the Jurassic and the Mesozoic (Figure 9). According to  
424 these reconstructions, the oceanic crustal segment that we have identified in the Gulf of Cadiz

425 would represent the last remnant of the western Alpine-Tethys lithosphere and, therefore, it  
426 would be one of the oldest oceanic crustal fragments currently preserved on Earth. It is  
427 interesting to note that the oceanic spreading would have mainly occurred during the so-called  
428 “Jurassic Quiet Zone” (Larson and Hilde, 1975), which would also explain the absence of a  
429 clear magnetic anomaly pattern in the area (e.g. Verhoef et al., 1991) despite its oceanic  
430 crustal nature.

431 In this context, we suggest that the large, prominent, south-dipping, low-velocity  
432 anomalies of figure 6 could be related with the presence of faults created during this rifting  
433 episode. Our interpretation is that they represent a smeared, coarse image of either the  
434 fractured, altered and fluid-saturated zone surrounding the fault area, or the contrast between  
435 rocks with different properties at both sides of the faults. According to our interpretation, f2  
436 and f3 would correspond to extensional faults generated during this phase, whereas f1 (and  
437 possibly f0) could represent either normal faults created during oceanic spreading or fracture  
438 zones. As we explained above, f0 and f1 coincide spatially with the two northernmost “SWIM  
439 lineaments”, whereas f2 coincides with a south-dipping fault reaching the seafloor that  
440 spatially coincides with the one imaged along MCS profile Voltaire-3 in the southern flank of  
441 the “Guadalquivir basement high” (see figure 9 in Terrinha et al., 2009). To our knowledge,  
442 there are no MCS data crossing the f3 anomaly (figure 6), so there is no link between this  
443 anomaly and other faults in the area. Finally, it is worth noting that f2 and f3 are imaged up to  
444 13-14 km and no deeper, this is near the base of the upper crust in the Variscan belt  
445 (Palomeras et al., 2009). This depth corresponds to the maximum expected depth for  
446 continental earthquakes, which is believed to be associated with a thermal limit that marks the  
447 transition between “brittle” upper crust and “ductile” lower crust (e.g. Scholz, 1988).

448

449 ***5.3. Implications for regional geodynamic models***

450 Different models have been proposed to date to explain the different geological, geophysical  
451 and geochemical observations of the Gibraltar arc-Alboran basin system, including past or  
452 present collision of continental lithosphere combined with lithospheric recycling either by  
453 convective removal (Platt and Vissers, 1989; Calvert et al., 2000), delamination (Seber et al.,  
454 1996), or slab break-off (Zeck, 1997); together with a variety of models of either continental  
455 or oceanic subduction with southward (Sanz de Galdeano, 1990; Morales et al., 1999),  
456 northward (Torres-Roldan et al., 1986; Mauffret et al., 2007), westward (Docherty and Banda,  
457 1995; Zeck, 1997), or eastward dips (Lonergan and White, 1997; Gutscher et al., 2002). The  
458 nature of the crust in the Gulf of Cadiz has important implications for these competing  
459 geodynamic models proposed for the SW Iberia region, especially for those proposing  
460 rollback of an eastward dipping subducted slab as the main driving force for the formation of  
461 the Alboran basin (Lonergan and White, 1997; Gutscher et al., 2002; Duggen et al., 2004;  
462 Faccenna et al., 2004).

463         Some authors had previously suggested the presence a 10-15 km-thinning of the  
464 Variscan continental crust in the central Gulf of Cadiz, based on land recordings of marine  
465 seismic data (González et al., 1996), modelling of gravity data (Gràcia et al., 2003), combined  
466 modelling of potential field data (Fernández et al., 2004; Zeyen et al., 2005), and joint  
467 geophysical and petrological modelling (e.g. Fullea et al., 2010). In contrast, our current  
468 findings evidencing the presence of oceanic crust in the central Gulf of Cadiz are fully  
469 compatible with the presence of a narrow, east-dipping, fast retreating oceanic slab beneath  
470 the Gibraltar arc. Our model and interpretation is also in agreement with available  
471 seismological data suggest the presence of a continuous, 150-200 km-wide slab that dips from  
472 the Gulf of Cadiz towards Gibraltar, reaching the 660 km-discontinuity beneath the Alboran  
473 basin. These data include the global tomography images showing a narrow subducted slab  
474 beneath Alboran and Gibraltar (e.g. Spakman and Wortel, 2004), the dispersion analysis of

475 body waves from the deep mantle indicating the presence of a steeply eastward dipping low  
476 P-wave waveguide within a high velocity slab (Bokermann and Mauffroy, 2007), and the  
477 recent shear-wave splitting measurements indicating a semicircular mantle flow pattern  
478 beneath the Gibraltar arc (Díaz et al., 2010).

479

## 480 **6. Conclusions**

481

482 Our WAS modelling results indicate the presence of three crustal domains in the SW Iberian  
483 margin. In the north, a 28-30 km-thick Variscan continental crust that gently thins to ~25 km  
484 beneath the coastline. Immediately South from it, a ~60 km-wide zone where almost all the  
485 crustal thinning (from ~25 km to ~7 km), concentrates. In the Southernmost part of the  
486 profile, a 150 km-wide segment of ~7 km-thick crust, overlain by a 1-2 km-thick lower unit of  
487 consolidated Mesozoic to Eocene sediments, and a 3-4 km-thick upper unit of sediments  
488 corresponding to the Upper Miocene GCIW that is covered in turn by a thin layer of plio-  
489 Quaternary sediments. The velocity gradient and crustal thickness in the southern section  
490 strongly suggests that the lithosphere is oceanic in nature, although absolute velocities are  
491 somewhat lower than “normal” probably due to fault-related rock fracturing and alteration  
492 and mantle serpentinization. The abrupt ocean-continent transition is suggested to be the  
493 result of the initial tectonics of the margin setting during the Triassic-early Jurassic as a  
494 transform margin, followed by oblique seafloor spreading between southern Iberia and north-  
495 western Africa during the Middle-Late Jurassic (roughly 180-145 Ma). According to our  
496 interpretation, the oceanic spreading that took place in the Jurassic would have generated a  
497 ~150 km-wide oceanic basin that would be part of the system that have once connected the  
498 Atlantic and Tethyan oceanic domains. Based on the spatial coincidence with previously  
499 identified active faults, we suggest that the wide, crustal-scale, south-dipping, low-velocity

500 anomalies imaged in the velocity model are the tomographic expression of the area affected  
501 by crustal-scale faults, some of which could have been created during this rifting period. The  
502 fragment of oceanic crust identified in the velocity model would therefore constitute the only  
503 remnant of the western Alpine-Tethys ocean and one of the oldest oceanic crustal fragments  
504 currently preserved on Earth. The presence of a narrow oceanic basin in the Gulf of Cadiz  
505 agrees with recent seismological observations, and it is consistent with the geodynamic  
506 models proposing roll-back of an eastward dipping slab as the main driving force for the  
507 opening of the Alboran Sea within the Betic-Rif system.

508

### 509 **Acknowledgments**

510

511 We thank the captain and crew of the research vessel BIO Hesperides, as well as the UTM  
512 and IFREMER technicians that were in charge of the airguns and OBS data acquisition. The  
513 NEAREST project has been funded by the the EU Programme “Integrating and Strengthening  
514 the European Research Area” of FP6, Sub-Priority 1.1.6.3, Global Change and Ecosystems”,  
515 contract n. 037110, and the NEAREST -SEIS survey was funded by the Complementary  
516 Action # CGL2006-27098-E/ BTE of the Spanish MICINN. Additional funds were obtained  
517 from the MICINN project MEDOC (CTM2007-66179-C02-02/MAR). We also acknowledge  
518 funding from MICINN through the Ramon y Cajal programme (R. Bartolomé). We finally  
519 acknowledge the collaboration of our research partners at Grup de Recerca de la Generalitat de  
520 Catalunya Barcelona Centre of Subsurface Imaging (B-CSI) ref. 2009 SGR 146 and funding  
521 support from Repsol-YPF.

522

523

523 **References**

524

525 Argus, D.F., Gordon, R.G., Demets, C., Stein, S., 1989. Closure of the Africa-Eurasia-North America  
526 plate motion circuit and tectonics of the Gloria fault, *J. Geophys. Res.* 94, 5585-5602.

527 Auffret, Y., P. Pelleau, F. Klingelhoefer, J. Crozon, J.Y. Lin, and J. C. Sibuet, 2004. MicroOBS: A new  
528 ocean bottom seismometer generation. *First Break*, 22, 41-47.

529 Auzende, J. M., et al., 1984. Intraoceanic tectonism on the Gorringe Bank: Observations by  
530 submersible, in *Ophiolites and Oceanic Lithosphere*, edited by I. G. Gass, S. J. Lippard, and A.  
531 W. Shelton, *Geol. Soc. Spec. Publ.*, 13, 113–120.

532 Banda, E., Torne, M., and the IAM Group, 1995. Iberian Atlantic Margins Group Investigates Deep  
533 Structure of Ocean Margins, a Multichannel Seismic Survey, *EOS* 76 (3), 25–29.

534 Bill, M., O’Dogherty, L., Guex, J., Baumgartner, P.O., Masson, H., 2001. Radiolarite ages in Alpine-  
535 Mediterranean ophiolites: Constraints on the oceanic spreading and the Tethys–Atlantic  
536 connection, *Geol. Soc. Am. Bull.*, 113, 129–43.

537 Bokelmann, G. and Maufroy, E., 2007. Mantle structure under Gibraltar constrained by seismic  
538 waveform complexity, *Geophys. Res. Lett.*, 34, L22305, doi:10.1029/2007GL030964

539 Buforn, E., Sanz de Galdeano, C., and Udias, A., 1995. Seismotectonics of the Ibero-Maghrebian  
540 region, *Tectonophysics*, 248, 247-261.

541 Calahorrano, A., V. Sallarès, J.-Y. Collot, F. Sage and C. R. Ranero, 2008. Structure and physical  
542 properties of the subduction channel off the Gulf of Guayaquil (Ecuador) from seismic reflection  
543 data, *Earth Planet. Sci. Lett.*, 267 (3-4), 453-467, doi:10.1016/j.epsl.2007.11.061

544 Calvert, A., Sandvol, E., Seber, D., Barazangi, M., Roecker, S., Mourabit, T., Vidal, F., Alguacil, G.,  
545 and Jabour, N., 2000. Geodynamic Evolution of the Lithosphere and Upper Mantle Beneath the  
546 Alboran Region of the Western Mediterranean: Constraints from Travel Time Tomography, *J.*  
547 *Geophys. Res.*, 105, 10,871-10,898.

548 Dañoibeitia, J.J., Bartolome, R., Checa, A., Maldonado, A., and Slootweg, A.P., 1999. An  
549 interpretation of a prominent magnetic anomaly near the boundary between the Eurasian and  
550 African plates (Gulf of Cadiz, SW margin of Iberia). *Marine Geology*, 155, 45-62.

551 Diaz, J., J. Gallart, A. Villaseñor, F. Mancilla, A. Pazos, D. Córdoba, J.A. Pulgar, P. Ibarra, M.  
552 Harnafi, and the TopoIberia Seismic Working Group, 2010. Mantle dynamics beneath the  
553 Gibraltar Arc (W Mediterranean) from shear-wave splitting measurements on a dense seismic  
554 array. *Geophys. Res. Lett.*, 37 (18), L18304, doi: 10.1029/2010GL044201.

555 Docherty, C., and E. Banda, 1995. Evidence for the eastward migration of the Alboran Sea based on  
556 regional subsidence analysis: A case for basin formation by delamination of the subcrustal  
557 lithosphere?, *Tectonics*, 14 (4), 804–818, doi:10.1029/95TC00501.

558 Duggen, S., Hoernle, K., van den Bogaard, P., Harris, C., 2004. Magmatic evolution of the Alboran  
559 Region: The role of subduction in forming the western Mediterranean and causing the Messinian  
560 Salinity Crisis. *Earth Planet. Sci. Lett.* 218, 91-108.

561 Faccenna, C., Becker, T.W., Lucente, F.P., Jolivet, L. and Rossetti, F., 2001. History of subduction  
562 and back-arc extension in the Central Mediterranean. *Geophys. J. Int.*, 145: 809-820.

563 Faccenna, C., Piromallo, C., Crespo-Blanc, A., Jolivet, L. and Rossetti, F., 2004. Lateral slab  
564 deformation and the origin of the western Mediterranean arcs. *Tectonics*, 23, 1-21.

565 Fernàndez, M., Marzan, I. and Torné, M., 2004. Lithospheric transition from the Variscan Iberian  
566 Massif to the Jurassic oceanic crust of the Central Atlantic. *Tectonophysics*, 386, 97-115.

567 J., Afonso, J.C., Fernàndez, M., and Vergés, J., 2007. A rapid method to map the crustal and  
568 lithospheric thickness, using elevation, geoid and thermal analysis. Application to the Gibraltar  
569 Arc System, Atlas Mountains and adjacent zones, *Tectonophysics*, 430, 97-117,  
570 doi:10.1016/j.tecto.2006.11.003.

571 Fullea, J., Afonso, J. C., Fernàndez, M., Vergés, J., Zeyen, H., 2010. The structure and evolution of  
572 the lithosphere - asthenosphere boundary beneath the Trans-Mediterranean region. *Lithos*, 120,  
573 74-95, doi: 10.1016/j.lithos.2010.03.003.



574 Gailler, A., Charvis, P., and Flueh, E.R., 2007. Segmentation of the Nazca and South American plates  
575 along the Ecuador subduction zone from wide-angle seismic profiles, *Earth Planet. Sci. Lett.*,  
576 260, doi: 10.1016/j.epsl.2007.05.045.

577 Girardeau, J., G. Cornen, M.O. Beslier, B. Le Gall, C. Monnier, P. Agrinier, G. Dubuisson, L.  
578 Pinheiro, A. Ribeiro, and H. Whitechurch, 1998. Extensional tectonics in the Gorringe Bank  
579 rocks, eastern Atlantic ocean: Evidence of an oceanic ultra slow mantellic accreting centre, *Terra*  
580 *Nova*, 10, 330–336.

581 González, A., Torné, M., Córdoba, D., Vidal, N., Matias, L.M., Díaz, J., 1996. Crustal thinning in the  
582 southwestern Iberia margin. *Geophys. Res. Lett.* 23, 2477–2480.

583 Gràcia, E., Danobeitia, J.J., Verges, J., Bartolome, R., 2003a. Crustal architecture and tectonic  
584 evolution of the Gulf of Cadiz (SW Iberian margin) at the convergence of the Eurasian and  
585 African plates. *Tectonics* 22, n.4, 1033, doi:10.1029/2001TC901045.

586 Gràcia, E., Danobeitia, J.J., Verges, J., PARSIFAL Team, 2003b. Mapping active faults offshore  
587 Portugal (36°N-38°N): Implications for seismic hazard assessment along the southwest Iberian  
588 margin. *Geology*, 31, 83-86.

589 Gràcia, E. and SWIM cruise party, 2006. Earthquake and Tsunami Hazards in the Southwest Iberian  
590 Margin: High-resolution imaging of active faults and paleoseismic signature at the external part  
591 of the Gulf of Cadiz . ESF EuroMargins SWIM Cruise Report (REN2002-11234-E-MAR), 46 pp

592 Grevemeyer, I., Kaul, N., and Kopf, A., 2008. Heat flow anomalies in the Gulf of Cadiz and off Cape  
593 San Vicente, Portugal. *Marine and Petroleum Geology*, doi:10.1016/j.marpetgeo.2008.08.006.

594 Grimison, N. L., and W. P. Chen, 1986. The Azores–Gibraltar plate boundary: Focal mechanisms,  
595 depths of earthquakes, and their tectonic implications, *J. Geophys. Res.*, 91(B2), 2029–  
596 2047. Gutscher, M.-A., Malod, J., Rehault, J.-P., Contrucci, I., Klingelhoefer, F., Mendes-Victor,  
597 L., Spakman, W., 2002. Evidence for active subduction beneath Gibraltar. *Geology* 30, 1071-  
598 1074.

599 Gutscher, M.-A., Malod, J., Rehault, J.-P., Contrucci, I., Klingelhoefer, F., Mendes-Victor, L., and  
600 Spakman, W., 2002. Evidence for active subduction beneath Gibraltar, *Geology*, 30, 1071– 1074

601 Gutscher, M.-A., Baptista, M.A., Miranda, J.M., 2006. The Gibraltar Arc seismogenic zone (part 2):  
602 constraints on a shallow east dipping fault plane source for the 1755 Lisbon earthquake provided  
603 by tsunami modeling and seismic intensity. *Tectonophysics*, Sp. Vol. "Natural laboratories on  
604 seismogenic faults", v. 427, p. 153-166, doi:10.1016/j.tecto.2006.02.025.

605 Gutscher, M.-A., Dominguez, S., Westbrook, G., Gente, P., Babonneau, N., Mulder, T., Gonthier, E.,  
606 Bartolome, R., Luis, J, Rosas, F., Terrinha, P., and the Delila and DelSis Scientific Teams.,  
607 2009a. Tectonic shortening and gravitational spreading in the Gulf of Cadiz accretionary wedge:  
608 observations from multi-beam bathymetry and seismic profiling. *Journal of Marine and*  
609 *Petroleum Geology*, Sp. Vol. on Submarine instabilities. doi:10.1016/j.marpetgeo.2007.11.008.

610 Gutscher, M.-A., Dominguez, S., Westbrook, G.K., and Le Roy, P., 2009b. Deep structure, recent  
611 deformation and analog modeling of the Gulf of Cadiz accretionary wedge: implications for the  
612 1755 Lisbon earthquake. *Tectonophysics Sp. Vol., Proc. of the MAPG Meeting Marrakech*  
613 *Morocco (guest editor D. Frizon de Lamotte)*., v. 475, p. 85-97, doi: 10.1016/j.tecto.2008.11.031.

614 Handy, M.R., Schmid, S., Bousquet, R., Kissling, E., Bernoulli, D., 2010. Reconciling plate-tectonic  
615 reconstructions of Alpine Tethys with geological-geophysical record of spreading and  
616 subductions in the Alps. *Earth Sci. Rev.*, doi:10.1016/j.earscirev.2010.06.002.

617 Hayes et al., 1974, DSDP Site 135 (Survey report), DSDP Volume XIV, doi:10.2973/  
618 dsdp.proc.14.1974

619 IOC, IHO and BODC, 2003. Centenary Edition of the GEBCO Digital Atlas, published on CD-ROM  
620 on behalf of the Intergovernmental Oceanographic Commission and the International  
621 Hydrographic Organization as part of the General Bathymetric Chart of the Oceans, British  
622 Oceanographic Data Centre, Liverpool, UK.

623 Iribarren, L., Verges, J., Camurri, F., Fullea, J., Fernandez, M., 2007. The structure of the Atlantic-  
624 Mediterranean transition zone from the Alboran Sea to the Horseshoe Abyssal Plain (Iberia –  
625 Africa plate boundary). *Marine Geology*, 243, 97-119. doi:10.1016/j.margeo.2007.05.011.

626 Ivandic, M., Grevemeyer, I., Berhorst, A., Flueh, E. R. and McIntosh, K., 2008. Impact of bending  
627 related faulting on the seismic properties of the incoming oceanic plate offshore of Nicaragua J.  
628 *Geophys. Res.*, 113 . B05410.

629 Johnston, A., 1996. Seismic moment assessment of earthquakes in stable continental regions - III New  
630 Madrid 1811–1812, Charleston 1886 and Lisbon 1755. *Geophys. J.Int.* 126, 314–344.

631 Korenaga, J., W. S. Holbrook, G. M. Kent, P. B. Kelemen, R. S. Detrick, H. C. Larsen, J. R. Hopper,  
632 and T. Dahl-Jensen, 2000. Crustal structure of the southeast Greenland margin from joint  
633 refraction and reflection seismic tomography, *J. Geophys. Res.*, 105, 21,591– 21,614

634 Larson, R. L., and T. W. C. Hilde, 1975. A Revised Time Scale of Magnetic Reversals for the Early  
635 Cretaceous and Late Jurassic, *J. Geophys. Res.*, 80 (17), 2586–2594, doi:10.1029/  
636 JB080i017p02586.

637 Lefeldt, M., Grevenmeyer, I., Goßler, J., and Bialas, J., 2009. Intraplate seismicity and related mantle  
638 hydration at the Nicaraguan trench outer rise, *Geophys. J. Int.*, 178 (2), 742-752.

639 Le Roy, P., and Piqué, A., 2001. Triassic–Liassic western Moroccan synrift basins in relation to the  
640 central Atlantic opening. *Marine Geology*, 172, 359–381,doi: 10.1016/S0025-3227(00)00130-4.

641 Lonergan, L. and N. White, 1997. Origin of the Betic-Rif mountain belt. *Tectonics* 16(3): 504-522.

642 Malod, J. A., and D. Mougenot, 1979. L'histoire géologique néogène du Golfe de Cadix, *Bull. Soc.*  
643 *Geol. Fr.*, XXI, 603 – 611.

644 Martinez-Solares, J.M., Lopez A., and Mezcua, J., 1979. Isoseismal map of the 1755 Lisbon  
645 earthquake obtained from Spanish data. *Tectonophysics* 53, 301-313.

646 Mauffret, A., Ammar, A, Gorini, C., Jabour, H. 2007. The Alboran Sea (Western Mediterranean)  
647 revisited with a view from the Moroccan Margin. *Terra Nova*, 19, 195–203.

648 Medialdea, T., Vegas, R., Somoza, L., Vázquez, J.T., Maldonado, A., Díaz-del-Río, V., Maestro, A.,  
649 Córdoba, D., Fernández-Puga, M.C., 2004. Structure and evolution of the “Olistostrome”  
650 complex of the Gibraltar Arc in the Gulf of Cadiz (eastern Central Atlantic): evidence from two  
651 long seismic cross-sections. *Mar. Geol.* 209, 173–198.

652 Meléndez, A., V. Sallarès, K. D. McIntosh, C. R. Ranero, 2009. Seismic structure of the Nicaraguan  
653 convergent margin by travel time tomographic inversion of wide-angle seismic data in the area of  
654 the 1992 Nicaragua slow earthquake, Abstract # T21C-1844, AGU General Meeting, San  
655 Francisco (USA).

656 Morales, J., Serrano, I., Jabaloy, A., Galindo-Zaldívar, J., Zhao, D., Torcal, F., Vidal, F., González-  
657 Lodeiro, F., 1999. Active continental subduction beneath the Betic Cordillera and the Alboran  
658 Sea. *Geology* 27, 735–738.

659 Moser, T. J., 1991. Shortest path calculation of seismic rays: *Geophysics*, 56, 59–67.

660 Nocquet, J.M., and Calais, E., 2004. Geodetic measurements of crustal deformation in the Western  
661 Mediterranean and Europe. *Pure Appl. Geophys.*, 161, 661-681.

662 Olivet, J.-L., 1996. La cinématique de la Plaque Ibérique, *Bull. Cent. Rech. Elf Explor. Prod.*, 20, 131-  
663 195.

664 Palomeras, I., Carbonell, R., Flecha, I., Simancas, F., Ayarza, P., Matas, J., Martínez-Poyatos, D.,  
665 Azor, A., González-Lodeiro, F., Pérez-Estaún, A., 2008. The Nature of the Lithosphere Across  
666 the Variscan Orogen of SW-Iberia: Dense Wide-Angle Seismic Reflection Data. *J. Geophys.*  
667 *Res.*, 114, B02302, doi:10.1029/2007JB005050

668 Platt, J.P., and Vissers, R.L.M., 1989, Extensional collapse of thickened continental lithosphere: A  
669 working hypothesis for the Alboran Sea and Gibraltar arc: *Geology*, v.17, p.540-543;

670 Purdy, G.M., 1975. The Eastern end of the Azores-Gibraltar plate boundary. *Geophys. J. R. Astr. Soc.*,  
671 43, 123–150.

672 Ranero, C. R., Phipps Morgan, J., McIntosh, K., Reichert, C., 2003. Bending, faulting and mantle  
673 serpentinization at the Middle America Trench. *Nature*, 425, 367-373.

674 Ranero, C. R. and Sallarès, V., 2004. Geophysical evidence for alteration of the crust and mantle of  
675 the Nazca Plate during bending at the north Chile trench, *Geology*, 32 (7), 549-552

676 Roeser, H. A., C. Steiner, B. Schreckenberger, and M. Block, 2002. Structural development of the  
677 Jurassic Magnetic Quiet Zone off Morocco and identification of Middle Jurassic magnetic  
678 lineations, *J. Geophys. Res.*, 107(B10), 2207, doi:10.1029/2000JB000094.

679 Roest, W. and Srivastava, S., 1991. Kinematics of the plate boundaries between Eurasia, Iberia, and  
680 Africa in the North Atlantic from the Late Cretaceous to the present, *Geology*, 19, 613–616.

681 Rovere, M., Ranero, C.R., Sartori, R., Torelli, L., and Zitellini, N., 2004. Seismic images and  
682 magnetic signature of Late Jurassic to Early Cretaceous Africa-Eurasia plate boundary off SW  
683 Iberia. *Geophysical Journal International*, 158, 554-568.

684 Ryan et al., 1973. Goringe Bank - Site 120 (Survey report), DSDP Volume XIII,  
685 doi:10.2973/dsdp.proc.13.1973

686 Sallarès, V., Ph. Charvis, E.R. Flueh and J. Bialas., 2003. Seismic structure of Malpelo and Cocos  
687 Volcanic Ridges and implications for hotspot-ridge interaction, *J. Geophys. Res.*, 108, B12, 2564,  
688 doi: 10.1029/2003JB002431

689 Sallarès, V., Ph. Charvis, E. R. Flueh, J. Bialas and the SALIERI Scientific Party, 2005. Seismic  
690 structure of the Carnegie ridge and the nature of the Galapagos hotspot, *Geophys. J. Int.*, 161 (3),  
691 763-788, doi: 10.1111/j.1365-246 X.2005.02592.x.

692 Sallarès, V. and C.R. Ranero, 2005. Structure and tectonics of the erosional convergent margin off  
693 Antofagasta, North Chile (23°30' S), *J. Geophys. Res.*, 110, B6, 6101, doi:  
694 10.1029/2004JB003418

695 Sanz de Galdeano, C., 1990. Geologic evolution of the Betic Cordilleras in the Western  
696 Mediterranean, Miocene to the present. *Tectonophysics*, 172, 107-119.

697 Sartori, R., Torelli, L., Zitellini, N., Peis, D., and Lodolo, E., 1994. Eastern Segment of the Azores-  
698 Gibraltar Line (Central-Eastern Atlantic): An Oceanic Plate Boundary with Diffuse  
699 Compressional Deformation, *Geology*, 22, 555–558.

700 Schettino, A., and Turco, E., 2011. Tectonic history of the western Tethys since the Late  
701 Triassic, *Geol. Soc. Am. Bull.*, 123 (1/2); 89–105, doi: 10.1130/B30064.1

702 Scholz, C.H., 1988. The brittle-plastic transition and the depth of seismic faulting, *Geol.*  
703 *Rundsch.*, 77 (1), 319-328.

704 Seber, D., Barazangi, M., Ibenbrahim, A., and Demnati, A., 1996. Geophysical evidence for  
705 lithospheric delamination beneath the Alboran Sea and Rif-Betic mountains. *Nature*, 379,  
706 785-790.

707 Spakman, W. and Wortel, R., 2004 A tomographic view on Western Mediterranean Geodynamics. In:  
708 The TRANSMED Atlas. The Mediterranean region from crust to mantle. Geological and  
709 Geophysical framework. Cavazza, W., Roure, F., Spakman, W., Stampfli, G., and Ziegler, P.  
710 (Eds.) *Episodes*, 27, 31-52.

711 Srivastava, S.P., Schouten, H., Roest, W.R., Klitgord, K.D., Kovacs, L.C., Verhoef, J. and Macnab,  
712 R., 1990. Iberian plate kinematics: a jumping plate boundary between Eurasia and Africa. *Nature*,  
713 344, 756-759.

714 Srivastava, S. P., Sibuet, J.-C., Cande, S., Roest, W.R. and Reid, I.D., 2000. Magnetic evidence for  
715 slow seafloor spreading during the formation of the Newfoundland and Iberian margins. *Earth*  
716 *Planet. Sci. Lett.*, 182, 61-76.

717 Stampfli, G.M., and Borel, G.D., 2002. A Plate Tectonic Model for the Paleozoic and Mesozoic, *Earth*  
718 *Planet. Sci. Lett.*, 196 (1-2) 17-33.

719 Stich, D., Ammon, C.J., Morales, J., 2003. Moment-tensor solutions for small and moderate  
720 earthquakes in the Ibero-Maghreb region. *J. Geophys. Res.* 108, 2148.

721 Stich, D., Serpelloni, E., Mancilla, F., Morales, J., 2006. Kinematics of the Iberia- Maghreb plate  
722 contact from seismic moment tensors and GPS observations. *Tectonophysics*, 426, 295-317.

723 Stich, D., Mancilla F.d.L., Pondrelli S., Morales, J., 2007. Source analysis of the February 12th 2007,  
724 Mw 6.0 Horseshoe earthquake : Implications for the 1755 Lisbon earthquake. *Geophys. Res.*  
725 *Lett.*, v. 34, L12308, doi :10.1029/2007GL030012.

726 Tarantola, A., 1987. *Inverse problem theory: Methods for data fitting and model parameter estimation*,  
727 Elsevier Science, New York, 613 pp.

728 Terrinha, P., Pinheiro, L.M., Henriot, J.-P., Matia, L., Ivanov, A.K., Monteiro, J.H., Akhmetzhanov,  
729 A., Volkonskaya, Cunha, M.R., Shaskin, P. and Rovere, M., 2003. Tsunamigenic-seismogenic  
730 structures, neotectonics, sedimentary processes and slope instability on the Southwest Portugese  
731 Margin. *Marine Geology*, 195, 55-73.

732 Terrinha, P., Matias, L., Vicente, J., Duarte, J., Luís, J., Pinheiro, L., Lourenço, N., Diez, S., Rosas, F.,  
733 Magalhaes, V., Valadares, V., Zitellini, N., Mendes-Víctor, L. and MATESPRO Team, 2009.  
734 Morphotectonics and Strain Partitioning at the Iberia-Africa plate boundary from multibeam and  
735 seismic reflection data. *Marine Geology*, 267, 3-4, 156-174.

736 Thiebot, E., and Gutscher, M.-A., 2006. The Gibraltar Arc seismogenic zone (part1): constraints on a  
737 shallow east dipping fault plane source for the 1755 Lisbon earthquake provided by seismic data,  
738 gravity and thermal modeling. *Tectonophysics Sp. Vol.* “Natural laboratories on seismogenic  
739 faults”, v. 427, p. 135-152, doi:10.1016/j.tecto.2006.02.024.

740 Toomey, D.R., and G.R. Foulger, 1989. Tomographic inversion of local earthquake data from the  
741 Hengill-Grensdalur central volcano complex, Iceland, *J. Geophys. Res.*, 94, 17,497-17,510.

742 Torelli, I., Sartori, R., Zitellini, N., 1997. The giant chaotic body in the Atlantic off Gibraltar: new  
743 results from a deep seismic reflection survey. *Marine and Petroleum Geol.*, 14, 125–138.

744 Torres-Roldan, R.L., Poli, G. and Pecerrillo, A., 1986. An early Miocene arc-tholeiitic magmatic dyke  
745 event from the Alboran Sea. Evidence for precollisional subduction and back-arc crustal  
746 extension in the westernmost Mediterranean. *Geol. Rundschau*, 75 (1), 219-234.

747 Tortella, D., Torne, M., Perez-Estaun, A., 1997. Geodynamic evolution of the eastern segment of the  
748 Azores–Gibraltar Zone: the Gorringe Bank and Gulf of Cadiz region. *Marine Geophys. Res.*, 19,  
749 211–230.

750 Verhoef, J., Collette, B. J., Danobeitia, J. J., Roeser, H. A., & Roest, W. R., 1991. Magnetic anomalies  
751 off West-Africa, *Mar. Geophys. Res.*, 13, 81-103.

752 White, R.S., McKenzie, D., O’Nions, R.K., 1992. Oceanic crustal thickness from seismic  
753 measurements and rare earth element inversions. *Journal of Geophysical Research*, 97, 19683-  
754 19715.

755 Zeyen, H., Ayara, P., Fernandez, M., and Rimi, A., 2005. Lithospheric structure under the western  
756 African-European plate boundary: a transect across the Atlas Mountains and the Gulf of Cadiz.  
757 *Tectonics*, 24, (TC2001), doi:10.1029/2004TC001639.

758 Zeck, H.P., 1997. Mantle peridotites outlining the Gibraltar Arc: Centrifugal extensional allochthons  
759 derived from the earlier Alpine, westward subducted nappe pile. *Tectonophysics*, 281, 195–207

760 Zitellini, N., Rovere, M., Terrinha, P., Chierici, F., Matias, L., and BIGSETS Team 2004. Neogene  
761 through Quaternary tectonic reactivation of SW Iberian passive margin. *Pure Appl. Geophys.*  
762 161, 565-587.

763 Zitellini, N., Gràcia, E., Matias, L., Terrinha, P., Abreu, M.A., DeAlteriis, G., Henriët, J.P.,  
764 Danobeitia, J.J., Masson, D., Mulder, T., Ramella, R., Somoza, L., and Diez, S., 2009. The quest  
765 for NWAfrica-SW Eurasia plate boundary west of Gibraltar. *Earth Planet. Sci. Lett.* v. 280, p. 13-  
766 50, doi :10.1016/j.epsl.2008.12.005.

767

767 **Figure Captions**

768

769 **Figure 1.-** Location map of the study area of the NEAREST-SEIS wide-angle seismic survey,  
770 including the two profiles that were acquired. Yellow circles display OBS and land stations  
771 locations along the N-S profile presented in this paper. The multi-beam bathymetry is a  
772 combination of the SWIM compilation (Zitellini et al., 2009) and GEBCO digital atlas (IOC  
773 et al., 2003). The different faults are taken from the NEAREST active faults map (Zitellini et  
774 al., 2009). White stars mark the location of DSDP sites 120 and 135. Inset: Global map  
775 including the major tectonic plates. Abbreviations: AB: Alboran Basin; AGFZ; Açores-  
776 Gibraltar Fault Zone; EUR: Eurasian plate, AFR: Africa/Nubia plate, IB: Iberia, BH:  
777 Basement High; CPS: Coral patch ridge, CPRF: Coral Patch Ridge fault, GF: Gloria Fault;  
778 GO: Gorringle bank, HAP: Horseshoe Abyssal Plain, HF: Horseshoe fault, LN: North SWIM  
779 lineament, LS: South SWIM lineament, PC: Portimao Canyon; SAP. Seine Abyssal plain,  
780 TAP: Tagus Abyssal Plain.

781

782 **Figure 2.-** Recorded seismic sections (up) and record sections with corresponding observed  
783 arrivals (grey circles with error bands) and calculated arrivals (white circles), corresponding  
784 to the vertical component of OBS32 (a), OBS37 (b), OBS41 (c), OBS44 (d) and land station #  
785 3 (d). Their corresponding locations along the profile can be seen in figure 1. The vertical axis  
786 represents reduced travel time (in seconds), and the vertical axis is offset (in km). Reduction  
787 velocity is 6 km/s. The white labels indicate the seismic phases that have been identified and  
788 modelled (see text for description). Short data gaps (white bands) are present in 3 OBS and  
789 the land station.

790



791 **Figure 3.-** Partial results at the different steps of the tomographic inversion procedure and ray  
792 tracing corresponding to the inverted seismic phases. White circles indicate OBS locations.  
793 Grey lines show the different geological boundary interfaces. (a) Resulting velocity model for  
794 the sedimentary layer. (b) Ray coverage of seismic phases used in the sedimentary layer  
795 inversion (Ps, PsP). (c) Resulting velocity model for the oceanic crust segment. (d) Ray  
796 coverage of seismic phases used in the oceanic crust inversion (Ps, Pg, PmP). (e) Resulting  
797 velocity model for the continental crust. (f) Ray coverage of seismic phases used in the  
798 continental crust inversion (Pg, PmP).

799

800 **Figure 4.-** 2-D final velocity model obtained by tomographic inversion of the whole data set,  
801 constituted by arrival times of Ps, PsP, Pg, PmP and Pn phases. White circles indicate OBS  
802 locations. Black lines show the sediment-basement and crust-mantle boundaries (i.e., Moho).  
803 The initial model used in the inversion is a combination of the models displayed in figure 3  
804 (see text for details).

805

806 **Figure 5.-** (a) Derivative weight sum (DWS), and (b) Velocity and Moho depth uncertainty  
807 corresponding to the mean deviation of the 250 Monte Carlo realizations (see text for details).  
808 White circles indicate OBS locations.

809

810 **Figure 6.-** Map of negative velocity anomalies along the velocity profile, which correspond to  
811 the difference between the model displayed in figure 4 and a laterally-smoothed version of the  
812 same model. The filter applied to smooth the model is a Gaussian one with a lateral  
813 correlation length of 20 km and a vertical correlation length of 0.5 km. f0, f1, f2, and f3  
814 indicate the location of the most prominent and continuous features in the model that are  
815 interpreted in the text. White circles indicate OBS locations.

816

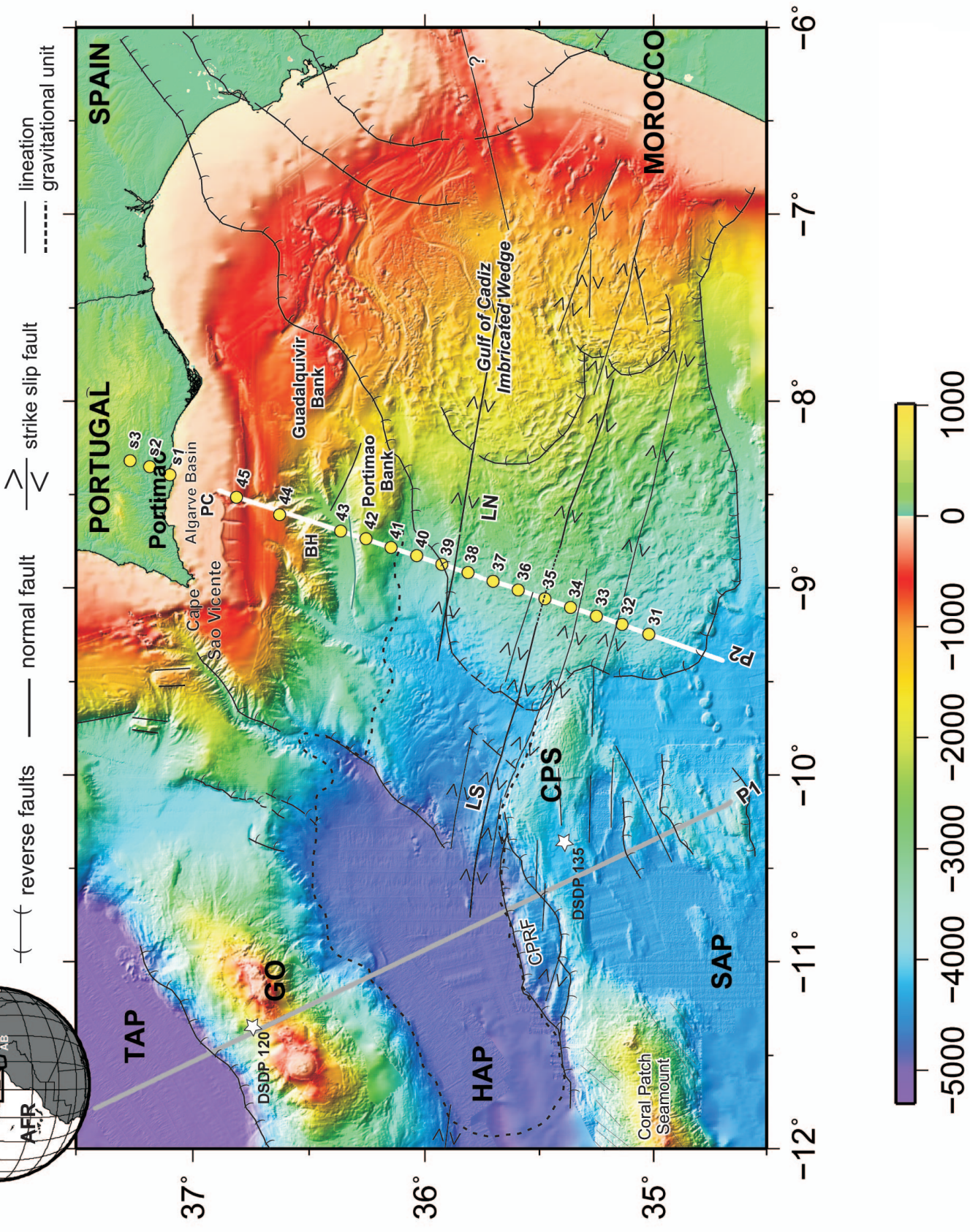
817 **Figure 7.-** Interpretative model of the structure and tectonics of the SW Iberian margin along  
818 the WAS profile displayed in figure 1. The different units and domains discussed in the text  
819 are indicated with the different colors. White circles indicate OBS locations. Abbreviations:  
820 f0, f1, f2, and f3 are faults; COB: Continent-Ocean Boundary, GCIW: Gulf of Cadiz  
821 imbricated wedge; LC: Lower Crust; UC: Upper Crust; BH: Basement High.

822

823 **Figure 8.-** 1-D P-wave velocity/depth profiles shown at three different locations along the  
824 WAS profile compared with compilations made for exhumed mantle, oceanic crust, and  
825 continental crust. (a) 1-D velocity-depth profile extracted at 60 km along the profile (P2,  
826 black line) and corresponding uncertainty bar (grey band), velocity profiles of exhumed  
827 mantle sections along the western Iberian margin (Iap, green line) and Tagus Abyssal plain  
828 (Tap, yellow line) (Srivastava et al., 2000), extended continental crust (ECC, brown area)  
829 (Christensen and Mooney, 1995), (b) 1-D velocity-depth profile extracted at 60 km along  
830 profile (P2, black line) and corresponding uncertainty bar (grey band), velocity profiles from  
831 Atlantic oceanic crust older than 140 m.y. (AOC, blue area) (White et al., 1992) and  
832 fractured, altered oceanic crust and serpentized mantle at the outer rise of the Nicaragua  
833 subduction zone (FOC, dark blue line with error band) (Meléndez et al., 2009), (c) 1-D  
834 velocity-depth profile extracted at 190 km along profile (P2, black line) and corresponding  
835 uncertainty bar (grey band), velocity profiles from AOC and ECC (see definition above), (d)  
836 1-D velocity-depth profile extracted at 190 km along profile (P2, black line) and  
837 corresponding uncertainty bar (grey band), velocity profiles from non-extended continental  
838 crust (CC, brown area) (Christensen and Mooney, 1995).

839

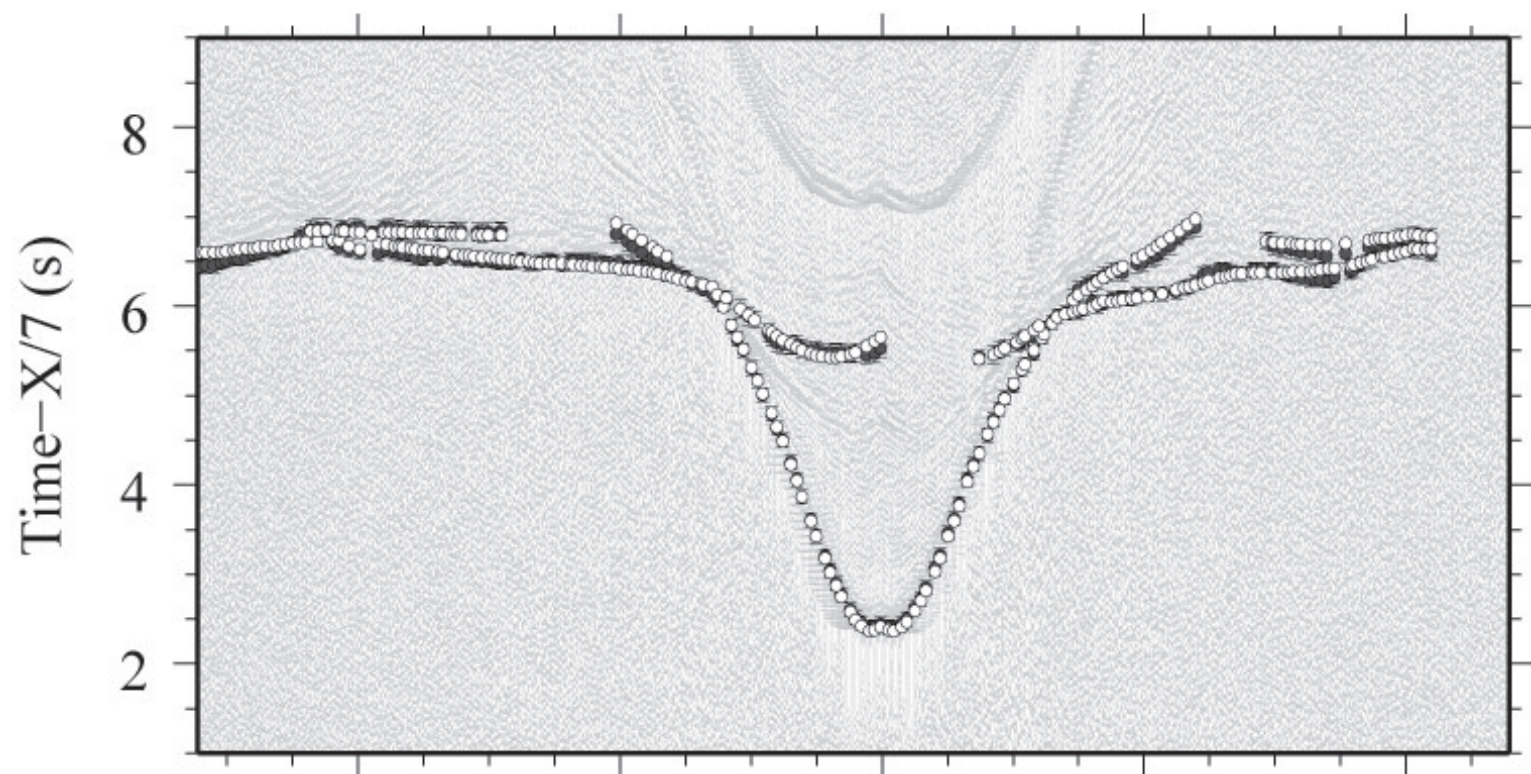
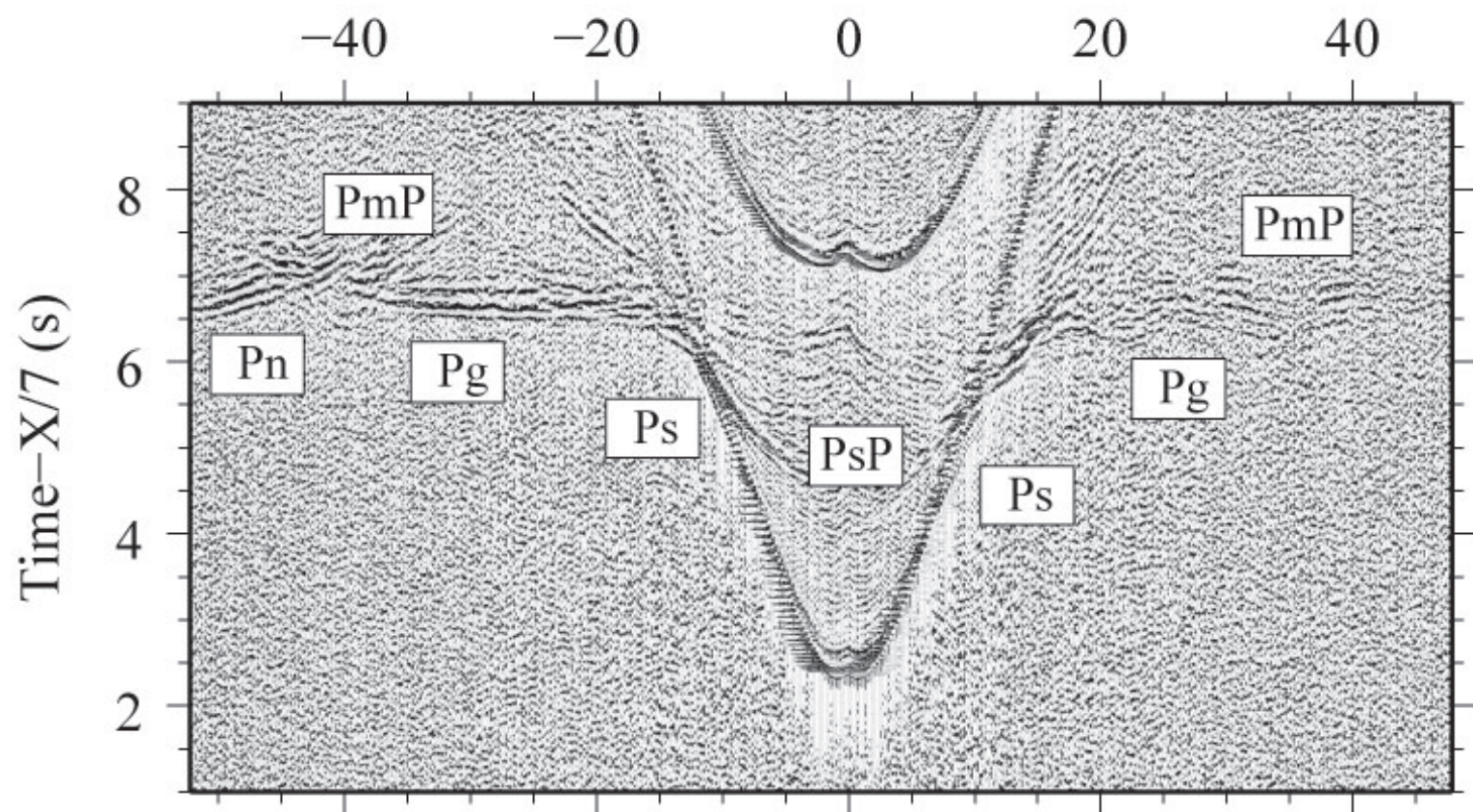
840 **Figure 9.-** Sketch summarizing our interpretation of the geodynamic and tectonic evolution  
841 between Eurasia/Iberia, Africa and north America during the Jurassic. The sequence includes  
842 (a) the initial phase of the ~E-W oceanic spreading at the Central Atlantic and the opening of  
843 the fracture zone, and (b) the initiation of oceanic spreading between Iberia and Africa to  
844 generate a series of narrow oceanic basins of oceanic crust connecting the Tethyan and  
845 Atlantic domains. Abbreviations: Bal: Balearic islands; Sar: Sardegna; Cor. Corsica; Adr:  
846 Adriatic; Apul: Apulia; Kab: Kabilie.





(a)

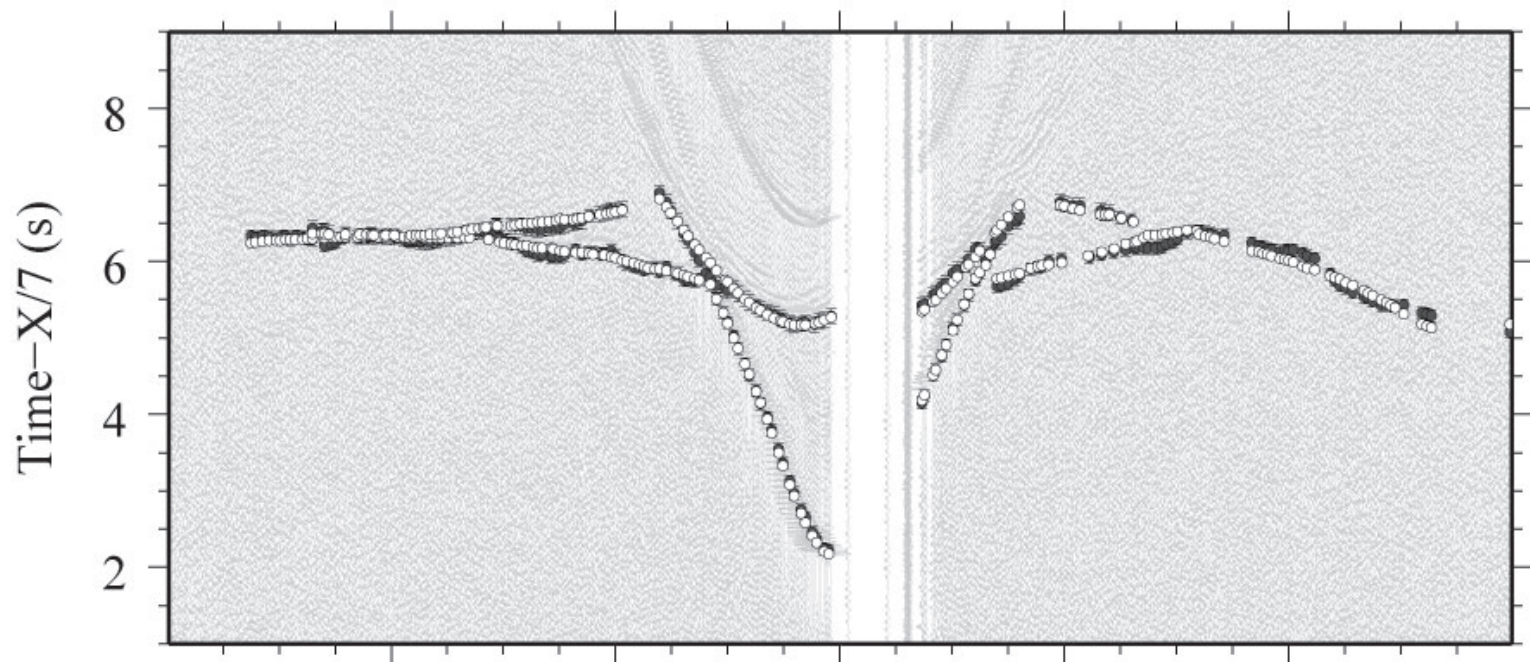
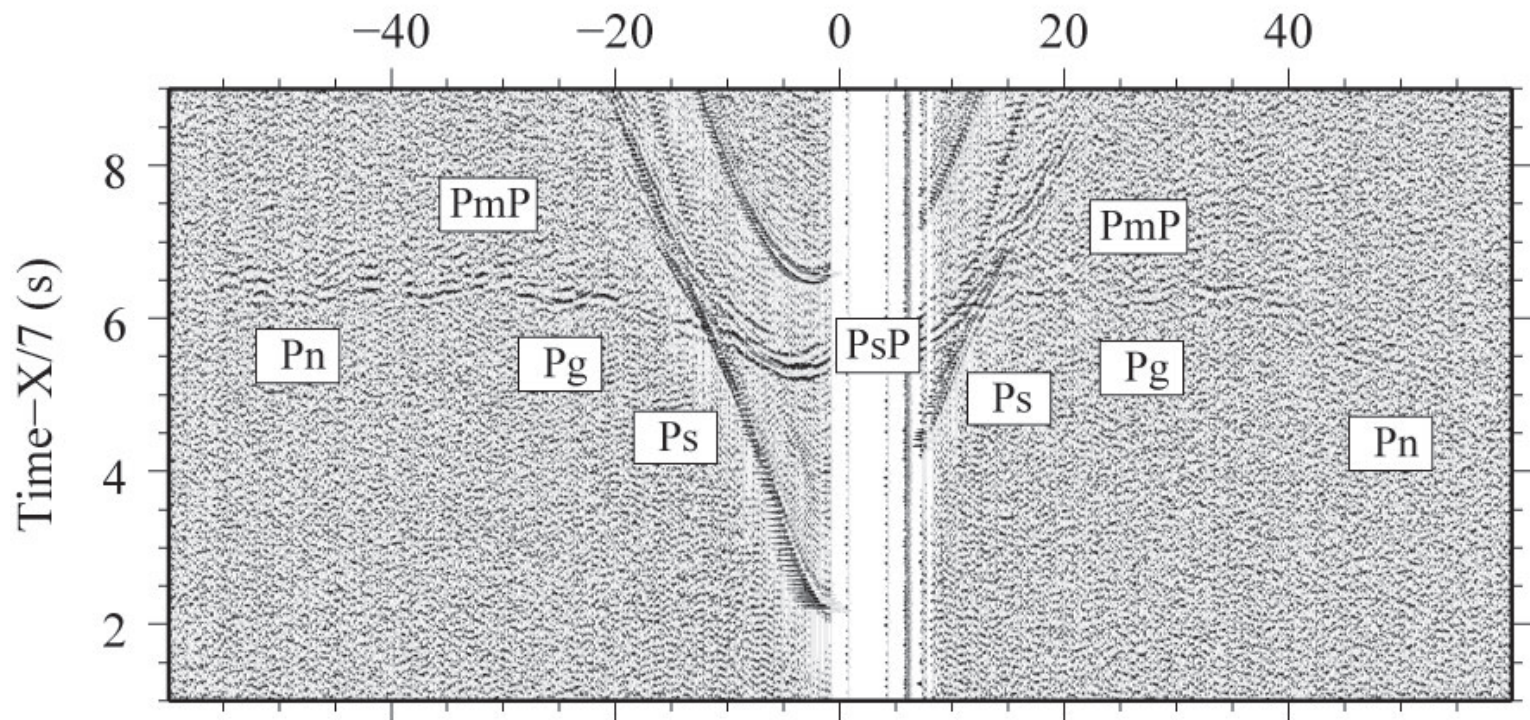
Offset From OBS32 (km)





(b)

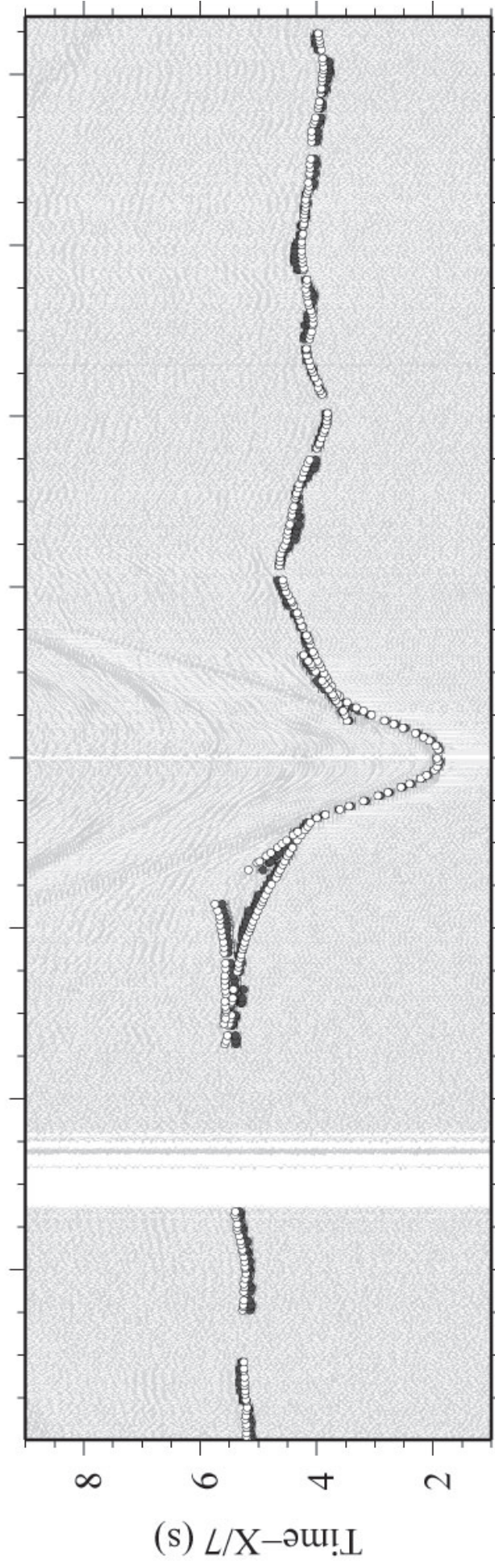
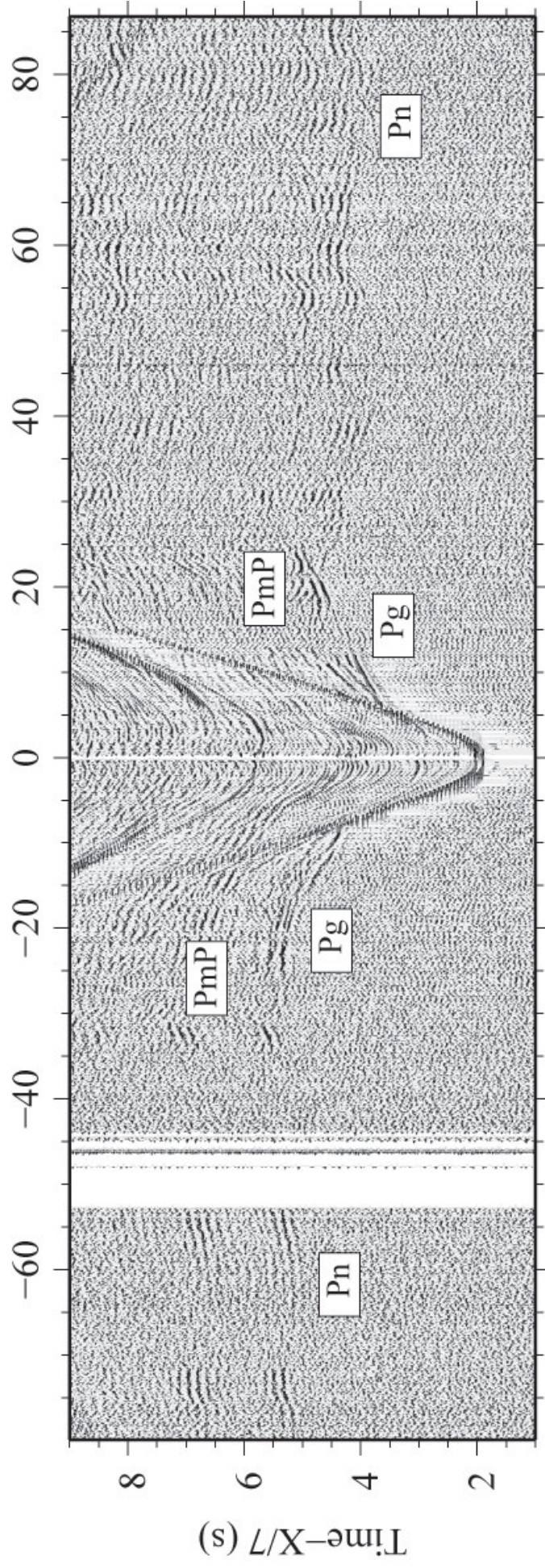
Offset From OBS37 (km)





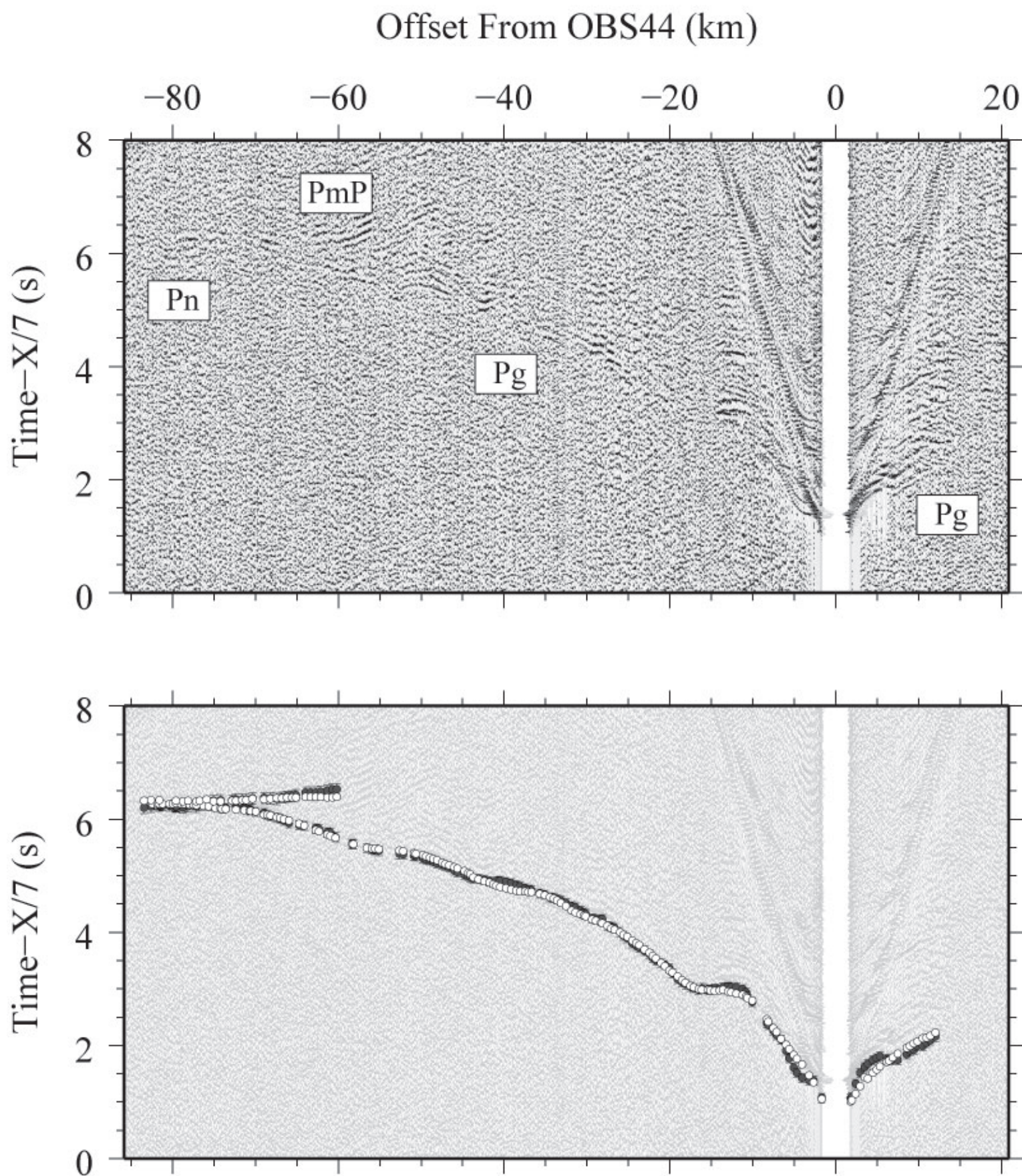
(c)

Offset From OBS41 (km)



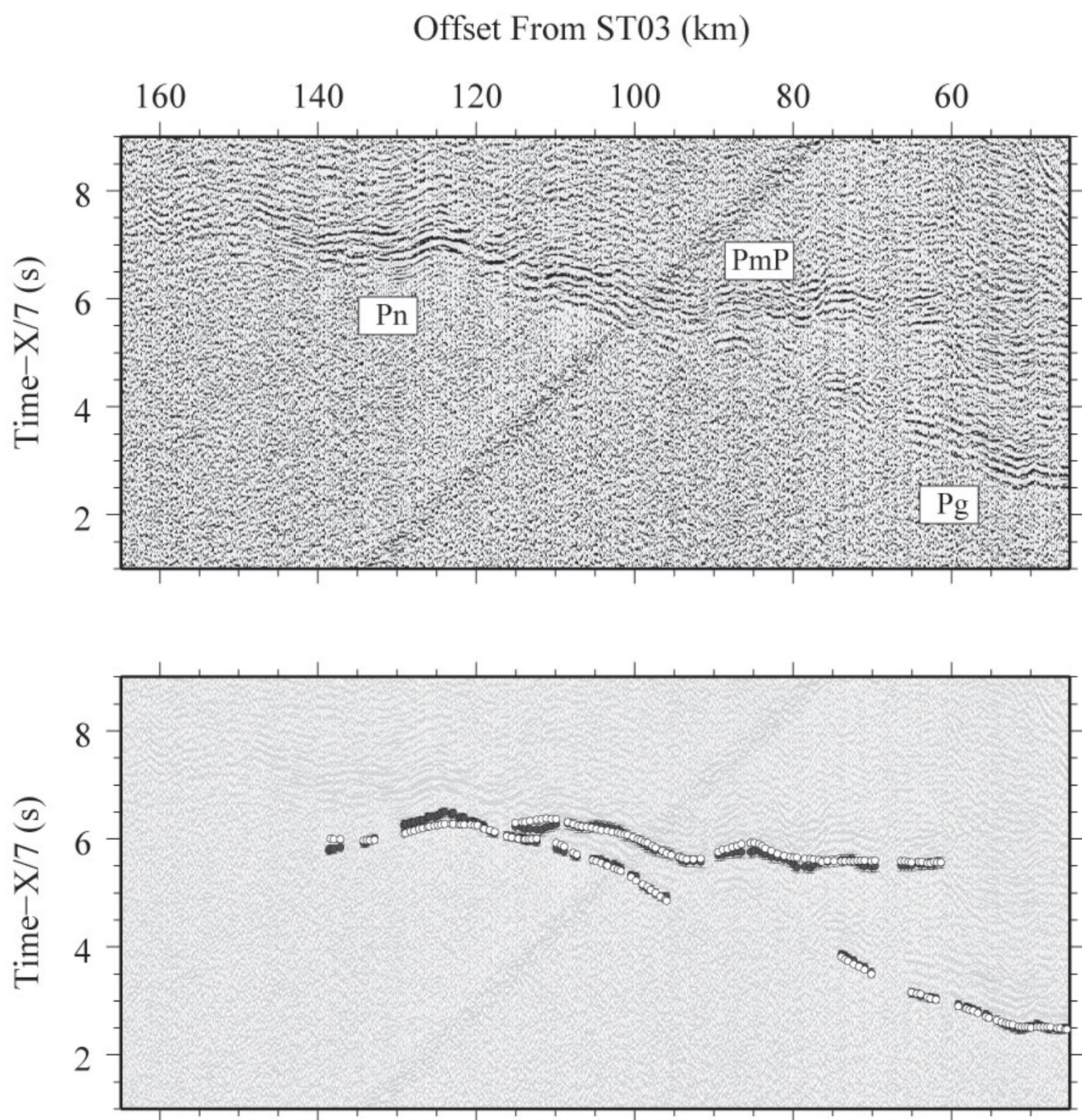


(d)

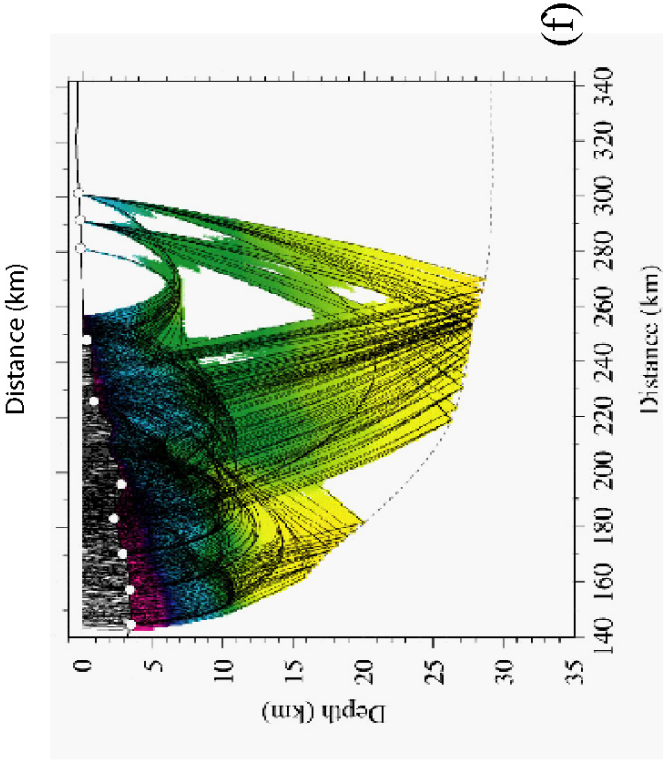
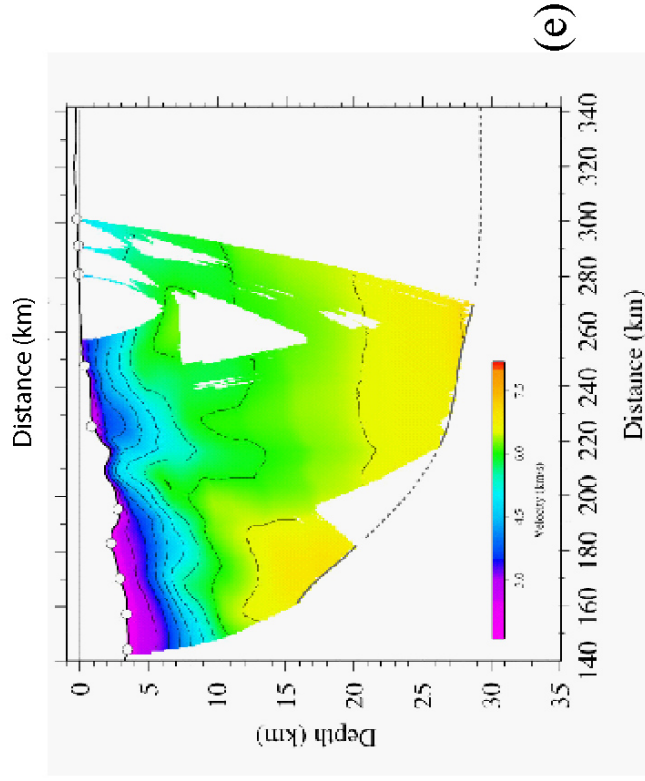
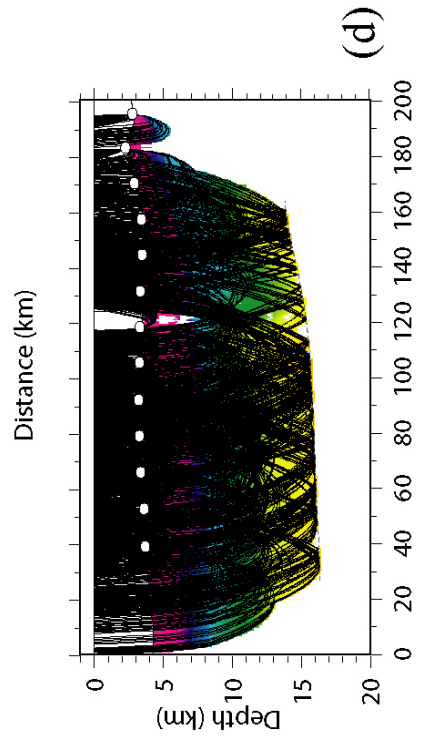
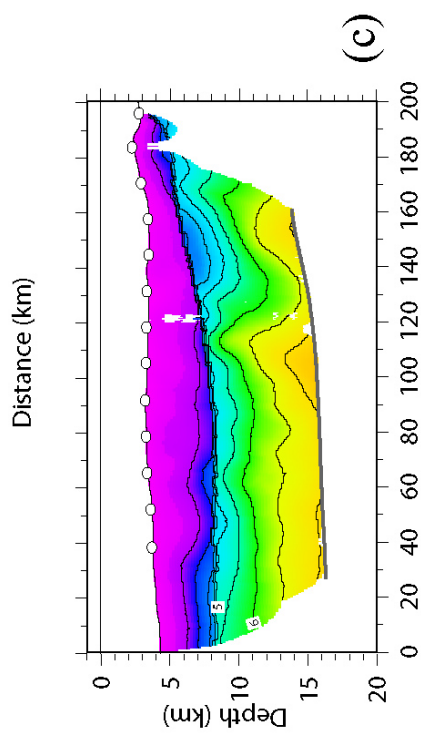
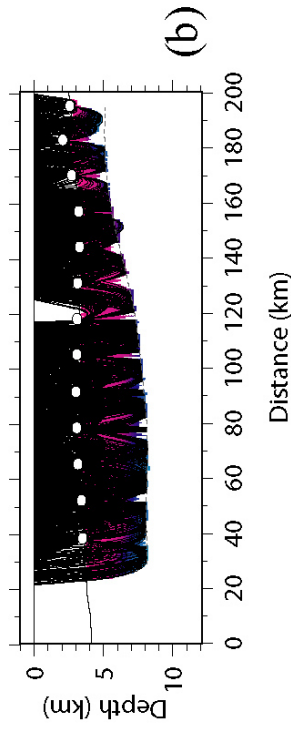
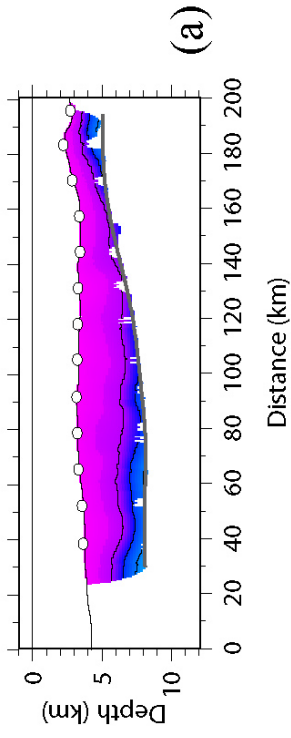


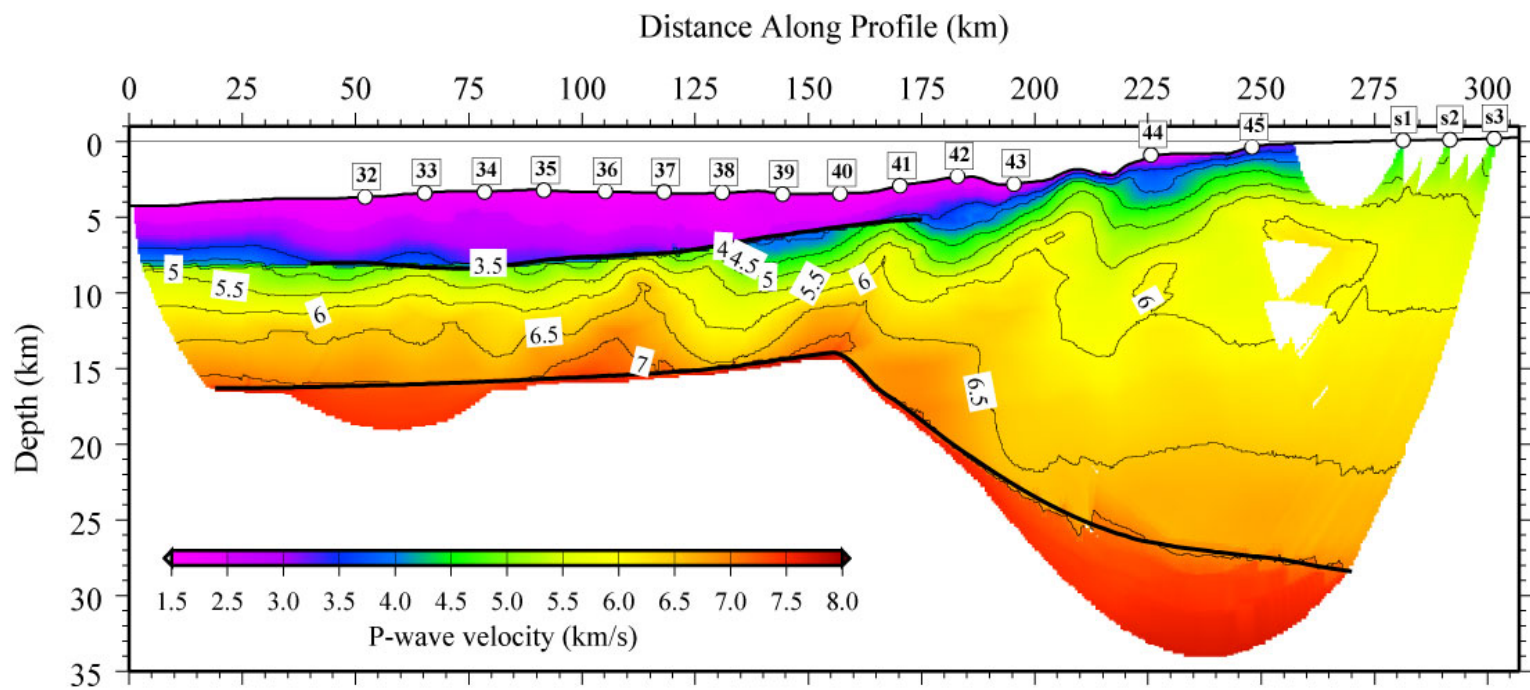


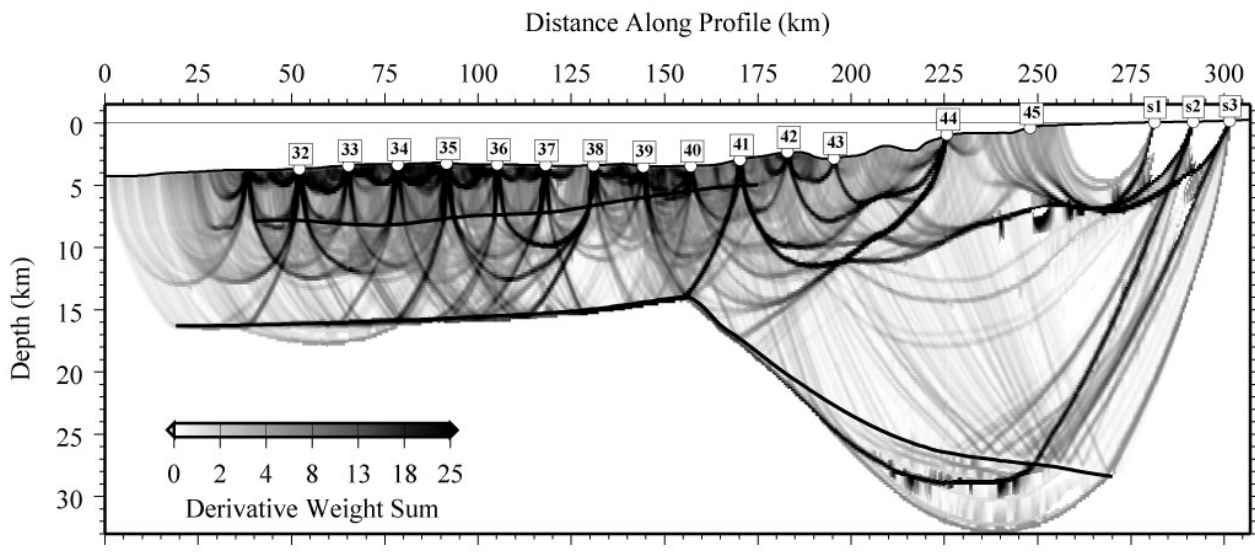
(e)



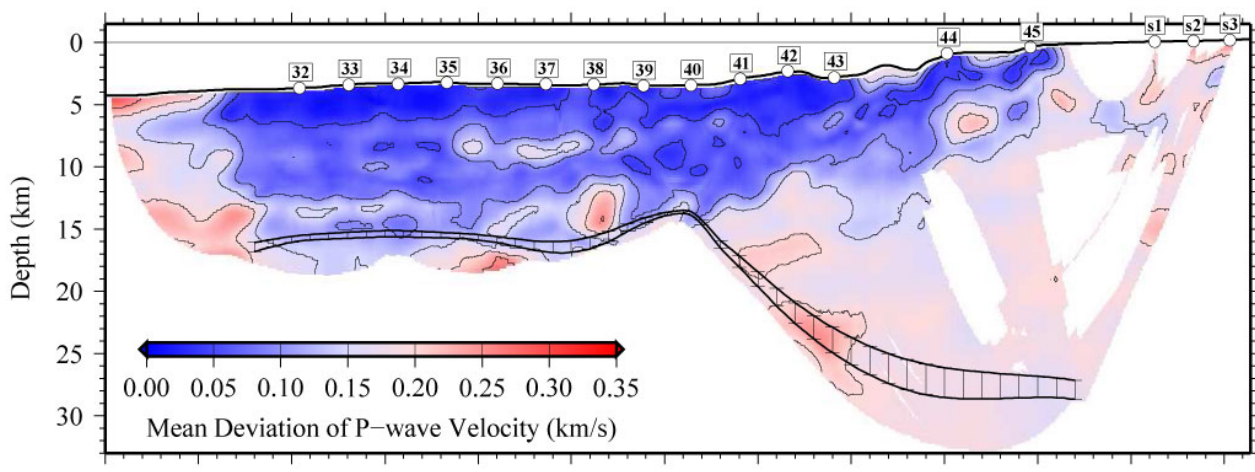








(a)



(b)

